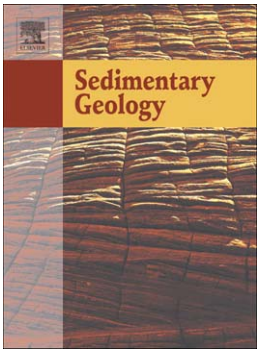

Sandy contourite drift in the late Miocene Rifian Corridor (Morocco): Reconstruction of depositional environments in a foreland-basin seaway

W. Capella, F.J. Hernández-Molina, R. Flecker, F.J. Hilgen, M. Hssain, T.J. Kouwenhoven, M. van Oorschot, F.J. Sierro, D.A.V. Stow, J. Trabucho-Alexandre, M.A. Tulbure, W. de Weger, M.Z. Yousfi, W. Krijgsman

PII: S0037-0738(17)30095-7
DOI: doi:10.1016/j.sedgeo.2017.04.004
Reference: SEDGEO 5186

To appear in: *Sedimentary Geology*

Received date: 7 February 2017
Revised date: 13 April 2017
Accepted date: 16 April 2017

Please cite this article as: Capella, W., Hernández-Molina, F.J., Flecker, R., Hilgen, F.J., Hssain, M., Kouwenhoven, T.J., van Oorschot, M., Sierro, F.J., Stow, D.A.V., Trabucho-Alexandre, J., Tulbure, M.A., de Weger, W., Yousfi, M.Z., Krijgsman, W., Sandy contourite drift in the late Miocene Rifian Corridor (Morocco): Reconstruction of depositional environments in a foreland-basin seaway, *Sedimentary Geology* (2017), doi:10.1016/j.sedgeo.2017.04.004

Sandy contourite drift in the late Miocene Rifian Corridor (Morocco): reconstruction of depositional environments in a foreland-basin seaway

W. Capella[1], F. J. Hernández-Molina[2], R. Flecker[3], F. J. Hilgen[1], M. Hssain[4], T.J. Kouwenhoven[1], M. van Oorschot[1], F. J. Sierro[5], D.A.V. Stow[6], J. Trabucho-Alexandre[1], M. A. Tulbure[1], W. de Weger[1], M.Z. Yousfi[4], W. Krijgsman[1]

[1] *Department of Earth Sciences, Utrecht University, 3584CD, Utrecht, the Netherlands*

[2] *Department of Earth Sciences, Royal Holloway, University of London, Egham, TW20 0EX, UK*

[3] *BRIDGE, School of Geographical Sciences and Cabot Institute, University of Bristol, Bristol, BS8 1SS, UK*

[4] ONHYM, 10050, Rabat, Morocco

[5] *Department of Geology, University of Salamanca, 37008, Salamanca, Spain*

[6] *IPE, Heriot-Watt Univ., Edinburgh EH14 4AS, Scotland, UK*

Abstract

The Rifian Corridor was a seaway between the Atlantic Ocean and the Mediterranean Sea during the late Miocene. The seaway progressively closed, leading to the

Messinian Salinity Crisis in the Mediterranean Sea. Despite the key palaeogeographic importance of the Rifian Corridor, patterns of sediment transport within the seaway have not been thoroughly studied.

In this study, we investigated the upper Miocene sedimentation and bottom current pathways in the South Rifian Corridor. The planktic and benthic foraminifera of the upper Tortonian and lower Messinian successions allow us to constrain the age and palaeo-environment of deposition. Encased in silty marls deposited at 150-300 m depth, there are (i) 5 to 50 m thick, mainly clastic sandstone bodies with unidirectional cross-bedding; and (ii) 50 cm thick, mainly clastic, tabular sandstone beds with bioturbation, mottled silt, lack of clear base or top, and bi-gradational sequences. Furthermore, seismic facies representing elongated mounded drifts and associated moat are present at the western mouth of the seaway.

We interpret these facies as contourites: the products of a westward sedimentary drift in the South Rifian Corridor. The contourites are found only on the northern margin of the seaway, thus suggesting a geostrophic current flowing westward along slope and then northward. This geostrophic current may have been modulated by tides. By comparing these fossil examples with the modern Gulf of Cadiz, we interpret these current-dominated deposits as evidence of late Miocene

Mediterranean overflow into the Atlantic Ocean, through the Rifian Corridor. This overflow may have affected late Miocene ocean circulation and climate, and the overflow deposits may represent one of the first examples of mainly clastic contourites exposed on land.

Key words: Marine gateway; marine sediments; sandstones; dune structures; contourites; Mediterranean Overflow Water.

1. Introduction

The Rifian Corridor was one of several relatively deep seaways that connected the Atlantic Ocean and the Mediterranean Sea during the late Miocene (Fig. 1). Its tectonic evolution resulted in a complex but generally asymmetric geometry, with deeper waters in the south. The Rifian Corridor was progressively uplifted at the end of the Miocene and its closure contributed to the isolation of the Mediterranean Sea (Flecker et al., 2015). Eventually, the Mediterranean Basin became disconnected altogether, sequestered ~10% of the world's ocean salt, and underwent repeated evaporation and desiccation during the Messinian Salinity Crisis (Roveri et al., 2014, and references therein). Uplift of the Betic-Rif arc (Fig. 1) resulted in the exposure of sedimentary remnants of the Rifian Corridor across the foreland of the Rif Mountains. These fossil remnants are upper Tortonian and lower Messinian mainly clastic

deposits and represent prime examples for the study of sedimentation in deep seaways.

Previous studies of sedimentary deposits of ancient seaways have mostly focussed on shallow seaways. Shallow (<100-150 m water depth) seaways display a range of bedforms created under the action of oceanic-, tidal-, and wind-currents, often resulting in a complex interplay of processes (e.g., Surlyk and Noe-Nygaard, 1992; Anastas et al., 1997; 2006; Olariu et al., 2012; Longhitano, 2013; Longhitano et al., 2014). This interplay of processes is unique to this environment, as the constricted morphology of the seaway acts to funnel and amplify the currents that shape the seafloor (Anastas et al., 2006; Longhitano, 2013).

By contrast, there are relatively few examples of ancient deep seaways and their deposits in the literature. Deep (> 150 m water depth) seaways are better known from oceanographic studies of modern systems (e.g., Denmark Strait, Iceland-Scotland ridge, Drake Passage, Gibraltar Strait; Swift, 1984; Mauritzen, 1996; Livermore et al., 2005; Scher and Martin, 2006; Legg et al., 2009; Hernández-Molina et al., 2014b), which show that deep seaways are commonly dominated by bottom-currents related to permanent ocean currents. In deep seaways, the bottom-current speed can be influenced by tectonically-created sills that separate landlocked basins from open oceans (Legg et

al., 2009). The constriction allows flow acceleration through the sill and dense gravity bottom currents, known as overflows, form (Legg et al., 2009; Rogerson et al., 2012; Rebesco et al., 2014).

In the Rifian Corridor, it remains unclear which processes controlled bottom-currents and sediment transport. In the intramontane basins forming the northern arm (Fig. 1), sandstone-marlstone alternations show an east to west pattern of progradation of the coarser sediments (Wernli, 1988). Further east, cross-stratified sandstones overlie upper Tortonian marine marls at Arbaa Taourirt (Fig. 1) and have been suggested to reflect the inflow of Atlantic water into the Mediterranean Sea (Achalhi et al., 2016). In the southern arm of the seaway (Fig. 1), nearly all sedimentological information is either extracted from stratigraphic works (Guercif Basin; Krijgsman et al., 1999; Gelati et al., 2000), or comes from internal reports focused on the provenance of siliciclastic sediments (Saiss and Gharb Basins; e.g., Cirac, 1987; Roksandic and Soquip, 1990; SCP/ERICO report, 1991). In the Gharb Basin, seismic data show turbiditic systems interrupted by channelised sedimentary drifts, possibly linked to bottom currents flowing west and out of the seaway (SCP/ERICO report, 1991; Fig. 2). The theoretical bottom-current patterns were brought into focus by a modelling study (de la Vara et al., 2015),

which showed that a two-layer, in- and out-flow exchange is possible and depends solely on the relative depth of the Betic and Rifian Corridors (Fig. 1). In the Rifian Corridor, neodymium isotopes record (Ivanovic et al., 2014) suggests that Mediterranean water reached the western end (Rabat sections) until ca.6.64 Ma.

It is the objective of this paper to improve our understanding of sedimentary processes and bottom-currents pathways in the southern arm of the late Miocene Rifian Corridor. We present three examples of the Rifian Corridor remnants, two of which comprise parallel and cross-stratified sandstones that we interpret as deposited by bottom currents. The third example is dominated by turbidites and related facies. These mainly clastic sandy contourites provide a very important ancient outcrop analogue for better understanding their nature and potential for hydrocarbon exploration (see Rebesco et al., 2014, for a discussion). Results are integrated with regional tectonic constraints to evaluate their implications for late Miocene palaeogeography and Mediterranean-Atlantic circulation.

2. Geological setting

The Rifian Corridor (Fig. 1) evolved as an underfilled foreland basin (*sensu* Crampton and Allen, 1995; Sinclair, 1997; Mutti et al., 2003) during the latest stage of collision of the Betic-Rif arc. It was a body of water

overlying the thrust-sheets at a time when they were already mostly emplaced (Frizon de Lamotte, 1979; Feinberg, 1986; Wernli, 1988, Capella et al., 2017). Westward convergence of the Alboran plate coupled with the Africa-Iberia collision formed the Betic-Rif arc (Platt et al., 2003; Vergés and Fernandez, 2012; Fig. 1). Thrust-sheets composed of deep-marine sediments (flysch and marls) were piled on top of the African margin to form the Rif external zones (Chalouan et al., 2008). Once established, the seaway was limited northwards and southwards by the earlier exhumed Rif orogenic wedge (Iribarren et al., 2009) and Atlas Mountains (Barbero et al., 2011), respectively (Fig. 1A).

Rifian Corridor sedimentation started at ca.8 Ma and was characterised by grey and blue fossiliferous marl with variable terrigenous intercalations (Wernli, 1988; Krijgsman et al., 1999; Gelati et al., 2000; Hilgen et al., 2000, Dayja, 2002; 2005; Barhoun and Bachiri Taoufiq, 2008; Achali et al., 2016). Evidence for carbonate factories is abundant on the Mediterranean side of the seaway (e.g., Saint-Martin and Cornée, 1996; Münch et al., 2006), but scarcer in the central areas of the corridor, where published data are limited to the Gulf of Skoura, on the south-eastern margin of the Saiss Basin (Charrière and Saint-Martin, 1989; Saint-Martin and Charrière, 1989; Fig. 1). The Gharb, Saiss, and Guercif basins formed the southern arm of the Rifian Corridor

(see Flecker et al., 2015, for a review), which roughly follows the curved trend of the nappe-thrust front (Fig. 1B).

Palaeo-depth estimations in the marly successions in the Saiss and Guercif basins suggest that the seaway's maximum depth was 400-600 m during the late Tortonian (upper bathyal) and gradually shallowed to ~100 m by the early Messinian, shortly before closure (Krijgsman et al., 1999; Dayja, 2002). Lower Messinian shallow marine deposits are locally truncated by an erosional unconformity and overlain by Pliocene continental deposits (Wernli, 1988; Krijgsman et al., 1999, Gelati et al., 2000; Nachite et al., 2003). By contrast, in the Gharb Basin to the west, the Pliocene is still marine (Wernli, 1988; Van der Laan et al., 2006).

The study area of this paper is confined to the Saiss Basin, the eastern Gharb Basin and the Prerif Ridges (Fig. 1B). The Prerif Ridges comprise Mesozoic carbonates belonging to the African margin, which was exhumed along high-angle faults and lateral ramps (Zizi, 1996, 2002). Most of the uplift of these structures postdates the Rif orogen build-up and was controlled by faults trending NE-SW to ENE-WSW, roughly perpendicular to the axis of the seaway (Sani et al., 2007; Capella et al., 2017). Their uplift along the Beth River area and the Sidi Fili Fault (Fig. 2) across the Tortonian-Messinian boundary may have restricted

connectivity between the Saiss and the Gharb basins and brought about shallow-marine and lacustrine sedimentation in the Saiss Basin (Cirac, 1987; SCP/ERICO report, 1991). Similarly, uplift of the Taza Sill (Fig. 1B) may have controlled the Guercif Basin connectivity to the west and its final isolation from the Atlantic Ocean (Cirac, 1987; Gomez et al., 2000).

. 3. METHODS

3.1. Fieldwork

Most of the information and the data presented in this paper are from field observations made at the East Fes, Ben Allou, and Haricha sections (Fig. 2). These mainly clastic successions unconformably overlie the Rif external zones, and in one case (East Fes) also their foreland. There is no consensus in the literature on the formal stratigraphic subdivision into formations and units of the upper Miocene, post-orogenic cover. The upper Miocene 'Neogene post-nappe' succession (*sensu* Feinberg, 1986; Wernli, 1988) is sometimes referred to as blue marls (e.g., Benson et al., 1991; Krijgsman et al., 1999) or Blue Marl Formation (Sani et al., 2007, Ivanovic et al., 2014). The basal transgressive surface on the African margin (Fig. 3) is thought to be synchronous in the Rifian Corridor and occurring at ca. 8–7.80 Ma (Krijgsman et al., 1999; Hilgen et al., 2000; Dayja et al., 2005).

We constructed 8 detailed sedimentary logs, measured 220 palaeocurrent indicators in cross-stratified sandstones, identified facies and trace-fossil assemblages, collected 37 (25 Ben Allou; 2 El Adergha; 10 Haricha) samples in sandstone for thin-sections and porosity test. We collected 183 samples in marlstone, every 3-5 m where possible, to determine the biostratigraphic assemblages throughout the sections.

In addition to the field data, we consulted the seismic database of ONHYM (Office National des Hydrocarbures et des Mines) and we present a 2D multichannel reflection seismic line crossing the Haricha section and part of the Gharb Basin (Fig. 2). This seismic profile has been acquired in 1985 for mid-depth petroleum exploration targets; structures at depth, age, and lithology of the seismic units are based on a regional seismic network calibrated by wells (Roksandic and Soquip, 1990; SCP/ERICO report, 1991; ONHYM unpublished data). We focussed on the uppermost, post-orogenic cover. Seismic stratigraphic analysis followed basic and classic criteria from Payton et al. (1977), Hardage (1987), Emery and Myers (1996). Discontinuities and seismic units were identified thus characterising the major sedimentary stacking pattern changes. Sedimentary drifts in seismic facies are identified and interpreted following the criteria from

Faugères et al. (1999), Nielsen et al. (2008), and Rebesco et al. (2014).

3.2 Sedimentology

The measurement of palaeocurrent directions (n= 220) was carried out systematically in cross-bedded sets in the 3 sites. Cross-sets were classified following the criteria from Anastas et al. (1997) on the basis of internal organization (simple or compound – based on the presence of intra-set discontinuities), thickness of the sets (thin is < 40 cm; 40 < medium < 75 cm; 75 < thick < 500 cm; very thick is > 500 cm), foreset shapes (straight and sinuous), and the nature of the lower bounding surface (planar or trough-shaped). Because the data were acquired in deformed strata we corrected cross-bedding for tectonic tilt using the software *stereonet*. The data were then plotted using a non-linear frequency scale with $r_{1\%}$ = 1 cm (Nemec, 1988).

To characterise the sands, we determined the microfacies and dominant mineral components in 37 thin-sections, which were obtained in key stratigraphic positions. Thin sections were realised at the Department of Earth Science, RHUL (UK), and analysed through a Petrographic Microscope Nikon. Grainsize from the Haricha section was detected by laser diffraction at Utrecht University; at Ben Allou and El Adergha, grainsize was determined from the thin-sections. To

determine the porosity, saturation and caliper/buoyancy techniques (Anovitz and Cole, 2015; Lin et al., 2015) were carried out by the Geolabs Company.

3.3. Biostratigraphy

Sampling for biostratigraphy was carried out in the finer-grained muds/marls, interbedded with the sandstones. Using the well-established chronological framework of high-resolution biostratigraphy for the late Miocene (e.g., Sierro et al., 1993; Krijgsman et al., 1995; Sprovieri et al., 1996; Hilgen et al., 2000; Krijgsman et al., 2004), we improved the age-estimates of the basin sediments that were previously dated as undifferentiated upper Tortonian-Messinian (Suter, 1980; Wernli, 1988). A semi-quantitative analysis of the planktic foraminiferal marker species was carried out on the > 150 μm size fraction of the washed residue. Maximum-minimum ages of deposition are determined as result of the presence, relative abundance or absence of key planktic foraminifera species, namely, for the studied interval, *Neogloboquadrina acostaensis;* the keeled globorotaliids as *Menardella (Globorotalia) menardii* form 4 (here called *G. menardii* 4), form 5 *(*here called *G. menardii* 5*),* and *Globorotalia miotumida.* In addition, also the sinistral or dextral coiling direction of *N. acostaensis* and *Globorotalia scitula* were used to determine age intervals, as well as the presence of the inflated form of *G. scitula* called *Globorotalia suterae* (e.g., Sierro et al., 1985,1993;

Sprovieri et al., 1999; Hilgen et al., 2000; Krijgsman et al., 2004; Lourens et al., 2004). This biochronology is based on an assemblage-based concept of the marker species (e.g., Sierro et al., 1993; Hilgen et al., 1995; Sprovieri et al., 1996) whose first, last regular occurrence or coiling changes are tuned to the astronomical time-scale (e.g., Lourens et al., 2004; Hilgen et al., 2012).

3.4. Inferences at palaeodepth

The water-depth of deposition has been inferred based on the benthic foraminifera assemblages contained in the hemipelagic marls of the studied sections. The specific assemblages were associated to ranges of depth, depending on the relative abundance of species present, with known depth-distribution in the literature (e.g., Pérez-Asensio et al., 2012). All the washed residues contain transported material, which is evident from the poorly sorted grainsize and differential preservation of foraminifera. Therefore, quantitative palaeodepth estimates based on plankton-benthos ratios or transfer functions (e.g., Van der Zwaan et al., 1990; Hohenegger, 2005, as applied in Pérez-Asensio et al., 2012) cannot be applied here. Additional complicating factors are: (a) the configuration of the seaway differs from that of a passive margin shelf-slope profile and is controlled by the orogenic wedge; (b) benthic foraminifera respond to environmental factors such as food flux, oxygen and

substrate type rather than to water depth (e.g., Lutze and Coulbourn, 1984; Linke and Lutze, 1993; Jorissen et al., 1995); and (c) depth distributions are not fixed, and changes in faunal composition with depth are gradual rather than abrupt (e.g., Lutze, 1980; Saidova, 2008). These factors cause imprecision in depth estimates of tens of metres at least.

However, inferences on the depth of the environment of deposition can be based on benthic foraminiferal assemblages and marker species with known present-day depth distribution. There is some analogy with the present–day Gulf of Cadiz, where foraminiferal depth distributions deviate from 'equilibrium' passive margins (Schönfeld, 1997, 2002; Rogerson et al., 2011) and shelf assemblages have extended their depth range. Most Rifian Corridor samples contain both shallow-water species, predominantly occurring in littoral and shelf environments (e.g., *Ammonia, Elphidium* and *Rosalina* spp.; *Gavelinopsis praegeri*, *Hanzawaia boueana*, *Nonion fabum:* Schönfeld 2002; Murray, 2006; Rogerson et al., 2011; Dorst and Schönfeld, 2013), and deeper-water species, commonly found on the outer shelf and upper slope (e.g., *Cibicides ungerianus, Cibicides kullenbergi, Cibicidoides pachyderma, Planulina ariminensis, Sphaeroidina bulloides, Uvigerina peregrina*; e.g., Fontanier et al., 2002; Schönfeld, 2002, 2006). In these cases, the shallow-water species are considered to have

been transported downslope, and the deeper-water ones are used for palaeodepth estimates.

4. RESULTS

4.1 East Fes

The East Fes composite section is located in the eastern Saiss Basin, 10 km east of Fes, and it consists of three sections: Sidi Harazem, El Adergha, and Ain Kansera (Fig. 3). The section comprises upper Tortonian marlstone with localised occurrence of sand beds (Fig. 4). The Messinian is absent at East Fes, although El Adergha reaches the Tortonian/Messinian boundary (see section 4.2).

4.1.1. Sidi Harazem

Sidi Harazem consists mainly of sandstones and marlstones. This section stratigraphically overlies a ~80 m thick condensed transgressive unit which unconformably overlies the Mesozoic basement (Sidi Harazem core; Wernli, 1988).

Near the village of Sidi Harazem (Fig. 5A), the sequence continues in outcrop for ~60 m with intercalations of marlstone and sandstone (Figs. 3, 4A). The sandstone beds (Fig. 5B) are up to 4 m thick; they are commonly structureless with normal grading and composed of poorly to moderately sorted, medium to coarse sands. The sand grains consist of quartz, carbonate-coated grains, and bioclastic shell debris. The

bottom of the beds shows burrows, load-casts and linear sole-marks (Fig. 6A), from which palaeocurrents measurements were obtained (Fig. 4B). Locally, channel-like features are observed, 5-10 m in width and 1-2 m deep (Fig. 5B).

4.1.2. El Adergha

El Adergha consists of a lower, mud-rich part, and an upper, sand-rich part. Moving north and up-sequence from Sidi Harazem village (Fig. 5A), the sandstone beds pass into a succession of massive, fossil-rich blue marlstones (Fig. 5C). These blue marlstones are poorly exposed. Their thickness, calculated with triangulation, is estimated to be 700 m (Fig. 4).

The 4-7 m thick, cross-stratified sandstone bedsets of the upper part are separated by a marlstone interval that contains thinner (ca. 20-50 cm) sandstone beds (Figs. 5, 6) with abundant bioturbation. The sands are, in general, medium to coarse, and poorly sorted with a variable fraction of clay, silt and bioclasts. These sands differ from those of Sidi Harazem in having a higher bioclastic content, more carbonate cement, and common cross-stratification (Fig. 6C, D). The two larger sandstone bedsets consist of laterally continuous beds (Fig. 5C) forming broad west-verging clinoforms at the top (Fig. 5D). The clinoformal strata are internally cross-stratified or parallel laminated; the sets of cross-strata

vary in thickness between 2 and 50 cm (Fig. 6C-E). The thicker cross-strata contain mud-drapes (Fig. 6D), and mud rip-up clasts occur along the boundaries between planar-laminated beds. Palaeocurrent reconstruction from the dip direction of internal cross-strata and accretion surfaces indicates a broadly unidirectional sense of flow to the west (Fig. 4B).

The thinner sandstone beds are tabular and show broad bi-gradational sequences (Fig. 6E). In the sandy intervals (Fig. 6E), cross-lamination and horizontal lamination are locally present. Porosity values of the sandy interval are ~12%.The sandstone beds lack a sharp base or top.

4.1.3. Ain Kansera

Ain Kansera outcrops further north and is stratigraphically lower than El Adergha. The marly deposits of Ain Kansera (Figs. 3, 4A) rest unconformably on the orogenic wedge. The siliciclastic content of the marlstones increases upwards; the marlstones then grade into several sandstone beds 1 to 10 m thick composed of medium to coarse and very coarse sands (Fig. 5F). These sandstone beds contain hummocks and swales; they are bioturbated and rich in bioclasts, such as bivalve and barnacle fragments (Fig. 6F-G). As bioclasts increase in size and concentration towards the top of the bed, grading is locally inverse. These 1 to 10 m

thick sandstone beds alternate with marlstones that become gradually thinner and disappear towards the top, where the last two sandstone beds contain large (~2 m thick) clinoforms. The average dip-direction of n= 8 clinoforms is towards the east-southeast. Other palaeocurrent indicators resulting in a wide range of directions (Fig. 4B) were, measured in trough- and swaley-cross stratification.

4.1.4. Age and palaeo-water depth

In Sidi Harazem, assemblages are dominated by both sinistrally coiled *N. acostaensis* and *G. suterae*, while *G. menardii* 4 appears in low numbers. These assemblages suggest an upper Tortonian age, older than the Last Common Occurrence (LCO) of *G. menardii* 4 at 7.51 Ma. The occurrence of *G. suterae* throughout the section further constrains the age between 7.80 and 7.51 Ma. This age is consistent with the occurrence of dominantly sinistral neogloboquadrinids (Hilgen et al., 1995; Krijgsman et al., 1995).

Samples collected between Sidi Harazem and El Adergha correspond to the interval between LCO *G. menardii 4* (7.51 Ma) and First Common Occurrence (FCO) of *G. menardii 5* (7.35 Ma). This also fits with the presence of *G. scitula* group, including *G. suterae*; dominantly sinistral neogloboquadrinids; and lower abundance of *G. menardii* 4. In El Adergha, samples

below and between the two 4–7 m thick sandstone bedsets are characterised by the presence of *G. menardii* 5, implying an age between 7.35–7.25 Ma. The coexistence of *G. menardii* 5 with specimens of the *G. miotumida* group, whose FCO is at 7.25 Ma (Hilgen et al., 2000; 2012), occurs in one of the uppermost samples, indicating that the uppermost part of this section is earliest Messinian in age.

The Ain Kansera marlstones contain predominantly sinistral *N. acostaensis*, but dextral specimens are present. *G. menardii* 4 is more abundant in the lower part of the section, whereas the percentage of the *G. scitula* group, including abundant *G. suterae*, is higher in the upper part. Consequently, we assigned an age older than 7.51 Ma to the lower part of this section (older than LCO of *G. menardii* 4 at 7.51 Ma), whereas the upper part contains an assemblage characteristic of the interval between the LCO of *G. menardii 4* and the FCO *G. menardii* 5 (7.35 Ma).

Benthic foraminiferal assemblages of Sidi Harazem contain many species commonly found in upper bathyal environments (e.g., *C. kullenbergi, P. ariminensis, Siphonina reticulata, S. bulloides, Sigmoilopsis schlumbergeri, U. peregrina*). Based on these assemblages the depositional environment is estimated to be upper slope (water depths of 250-400 m). The

lower part of El Adergha yields a similar depth of deposition, but the upper part contains fewer slope taxa and relatively more species common in outer shelf environments (*C. ungerianus*, *C. pachyderma*, spiroplectamminids) suggesting a position at the upper slope–outer shelf, at estimated depths between 150-300 m. The Ain Kansera marls contain shelf species (*N. fabum*, *Cibicides lobatulus*, *Cibicidoides pseudoungerianus*, *H. boueana*, small lenticulinids), fewer planktic foraminifera and no species from slope environments. The depositional environment is inner shelf (50-100 m water depth).

4.2 Ben Allou

The ~200 m thick Ben Allou section is located at the northern margin of the Saiss Basin, 30 km WNW of Fes, where it unconformably lies above the frontal thrust of the Rif orogenic wedge (Fig. 2). In plan view (Fig. 8A), there are two sandstone intervals that can be clearly followed over an area of ~ 2 km^2: sandstone interval 1 (subdivided SI-1a and SI-1b) and sandstone interval 2 (SI-2). The two sandstone intervals are folded into a gentle synform and form laterally extensive exposures. One of the clearest exposures (Fig. 8C) reveals a broad, erosive channel-form displaying an ENE-WSW axis in SI-1, a width of around 50 m and incision depth of 15 m. From SI-1 to SI-2 the channel depocentre appears to shift ~500 m northward, as indicated by the location of

the greatest thicknesses for SI-1 and SI-U2 (blue arrows in Fig. 8A). The base of the channel on the southwest face of SI-1a shows that the erosional surface is immediately overlain by cross-bedded sets, without gravel lags or mud layers (Fig. 8D and supplementary Fig. 2A).

To encompass the two sandstone intervals and detect lateral variations, we logged a north-eastern (Ben Allou A) and a south-western sector (Ben Allou B; Fig. 8A). Sedimentation in both sectors starts with blue-grey marlstone which increases upwards in siliciclastic content (the log of Ben Allou A only shows the upper part of the basal marlstone). At Ben Allou B the basal marlstones are ~50 m thick and are overlain by two cross-stratified, sheeted sandstone intervals encased in marlstones and heterolithic facies (Fig. 7). Panoramic views of the cross-stratified sandstone intervals (Fig. 8B, E) suggest that the thickness of the muds between the two sandstone intervals varies throughout the section. Effectively, 10 m of mud-marl deposits separates SI-1b and SI-2 at Ben Allou A, and is 60 m thick at Ben Allou B (Fig. 7). In both logging transects, SI-1 and SI-2 are encased in silty muds or heterolithic facies (Fig. 7). SI-1 and SI-2 display horizontal surfaces defined by bedding planes and sequence boundaries (Fig. 8C). Some of the sand beds have a sheeted shape and constant thickness;

others change laterally resulting in different stacking patterns.

Cross-stratification planes are defined by variations in grain size, bio- and siliciclastic content, or glauconite vs quartz. Grain size ranges from fine/medium to very coarse sands, with poor to moderate sorting and estimated porosity varying between 6.4% and 13%. The mineralogy of the sands comprises quartz, calcareous bioclasts, and heavy minerals. The amount of glauconite in the sandstones varies between 1%–10%, and that of bioclasts between 1% and 70 %, so that some of the sandstones are actually calcarenites. Rare bioclasts can be up to 1–2 cm diametres; beds with relatively high and low concentrations of bioclasts are interbedded.

4.2.1. Sedimentary structures

It is possible to observe different orders of cross-stratification at Ben Allou, from cross-lamination to thick cross-bedding, and superposition of simple and compound cross-bedding forming cross-stratified successions. The grain size ranges from very fine to very coarse sands; cross-stratification is present throughout. Cross-laminations are in general faint, rarely preserved, or obliterated by bioturbation. Bioturbation is abundant and present at all levels of the cross-strata (Fig. 9F). Cross-bedding is very common, indicating an overall paleocurrent direction to the southwest (Fig. 7B). Small

sets of cross-bedding can either form individual sheeted horizontal beds (Fig. 9B), or be the building blocks of compound sets (Fig. 9A). Compound sets display concave down or straight internal discontinuities, set-thicknesses from 40 to 250 cm, straight to sinuous foresets, planar to sub-planar bounding surfaces (Fig. 9B, C). Set bounding surfaces are trough-shaped only at Ben Allou B in SI-1a (Fig. 10A).

SI-1a at Ben Allou B consists of two superposed cross-stratified successions, separated by the erosional surface shown in Figs. 8C and 10C. The lower bounding surface has a large channelized shape at outcrop scale (50 m wide and 15 m deep). The first cross-stratified succession is ~18 m thick, and starts with two thick compound cross-bedded sets (Fig. 10C) which pass upwards into alternations of thin and medium, simple and compound sets (Fig. 10A). At the top, the succession ends with medium to thick, trough-shaped sets (Fig. 10B). The succession immediately above is 20 m thick and comprises alternations of simple to compound, thin to thick sets with planar bounding surfaces and straight foresets (Figs. 7, 9E).

Within the successions of SI-1b and SI-2, there are kink-folds or conical features, 1–2 m wide and extending through 1–3 m of section. These we interpret as late-stage fluid escape structures (Fig. 9 E), but note that they may also have some structural control. In most

cases the fluid escape structures are capped by undeformed set bounding surfaces (Fig. 9 E). Bedding-plane dip directions (documented by the bounding surfaces of planar, laterally extensive cross-sets) change from 15° towards N70 to 15º–20° towards N200 between SI-1a and SI-1b, respectively (Fig. 7).

SI-1b consists of a cross-stratified succession encased in silty marlstones (Fig. 7) and merges with SI-1a to the northeast, at Ben Allou A (Fig. 8B). We interpret this as indicating the erosive down-cutting of SI-1b. At Ben Allou B, SI-1b outcrops only at one location in a river gully (supplementary Fig. 2C). The succession of SI-1b comprises 10 to 15 m of medium to thick compound sets with planar bounding surfaces and straight to sinuous foresets.

SI-2 consists of a cross-stratified succession, 15 to 30 m thick, which consists of simple to compound, thin to medium sets of cross-bedding. At Ben Allou B, it is composed of thick sets of cross-bedding reaching 0.5 m in thickness (Fig. 10D). Nested within these high order structures, it is possible to observe simple to compound, small to medium sets (supplementary Fig. 2B). The lateral equivalent of the high-order structures is planar cross-bedding that occurs towards the northwest (Fig. 8E), in thin to thick sets with mostly straight foresets (supplementary Fig. 2E).

Within the sandstone intervals, mud or mud-drapes are absent. Mud-deposition occurs above and below the sandstone intervals, in 10 to 20 m thick intervals of heterolithic facies, that consist of structureless to faintly cross-stratified sandstone alternated with mudstone (Fig. 11A). Mud layers are mm to cm thick, while sand layers are cm to dm thick. The bioclastic content of the sand varies from 1% to 50%. The heterolithic facies display wavy bounding surfaces (Fig. 11B); some sandstone beds preserve cross-strata and asymmetrical dunes (Fig. 11C) with mud draping the topography. Thin sets of cross-beds are present but rare, while wavy lamination, composed of cm thick layers of sand and mud, is common (Fig. 11D).

4.2.2. Age and palaeo-water depth estimation

The planktic foraminiferal assemblage suggests an age between 7.80 and 7.51 Ma (late Tortonian). The lower part of the section (below SI-1) is dominated by sinistrally coiled *N. acostaensis* and *G. scitula*, including specimens of *G. suterae*, which suggests a late Tortonian age, younger than 7.80 Ma. The presence of *Globigerinoides*, with typical specimens of *G. extremus*, also confirms a post 8.37 Ma, late Tortonian age (Sprovieri et al. 1996; F. Lirer, pers. comm.) The uppermost marlstones, above SI-2, yielded abundant *G. menardii 4*, indicating that the whole succession was deposited before 7.51 Ma.

The benthic foraminiferal assemblages suggest that the Ben Allou section was deposited in upper bathyal environments, roughly equivalent to the upper slope physiographic domain (250-400 m water depth). The species *P. ariminensis*, *S. bulloides*, *Uvigerina semiornata* and *U. peregrina* are present throughout, and *C. kullenbergi* occurs in about half of the samples. The upper part of the section contains less slope taxa, indicating a slightly shallower depth range (upper slope–outer shelf physiographic domain, 150–300 m water depth).

4.3 Haricha

The Haricha section is located in the easternmost Gharb Basin, 40 km north of Meknes. This section is the one of the best exposures of Messinian deep-water, sand-marl alternations in the Gharb Basin (SCP/ERICO report, 1991). It unconformably overlies the orogenic wedge and consists of alternations of marlstone, siltstone, and sandstone (Fig. 12). The distinct tilt of the section (35° to 45° to the west; Figs. 13 B, C) is associated with tectonic uplift of Mount Bou Draa (Fig. 2), which is the lateral ramp of the frontal thrust of the Prerif Ridges.

The lowermost ~100 m of the section consist of alternating sandstones and bioturbated siltstones or silty marlstones (Fig. 14A). Sandstone beds are purple-coloured, bioturbated (Fig. 14A) or massive to laminated

with bioturbated tops (*Rhyzocorallium*-type; Fig.14B). The siltstones are predominantly light to dark grey and contain variable quantities of mud and heavy minerals. The sandstones contain shell debris (e.g., bivalves and bryozoans), lack clear grading, and often appear structureless, although ~5 cm thick divisions of parallel- and cross-lamination are present locally (Fig. 14A). One hundred and fifty metres of marlstones separate the two sandstone intervals (Fig. 12). The marlstones contain a variety of fossils, mainly bivalves and echinoderms.

The uppermost 200 to 250 m thick part of the section (Fig. 12) comprises grey, silty marlstones interbedded with reddish sandstones. The sandstones show a slight fining-upward trend, with a sharp basal contact and a gradational to sharp upper contact. The thickness of the sandstone beds increases towards the top, as well as the occurrence of structureless and amalgamated beds. Almost all sheeted sandstone beds have relatively flat bases which are uneven and moderately erosional in places (Fig. 14C) and show linear sole-marks and load-casts (Fig. 14D), indicating a broad westward direction of flow (Fig. 12). Some beds show scoured bases or comprise sandy channel fills (Fig. 14C); bioturbation is common throughout (Fig. 14D, E). The sandstones consist of poorly to well-sorted, fine to medium sand. The sands consist mainly of subrounded to subangular quartz (~30%), lithic fragments (~20%), feldspar (~5%),

heavy minerals (~2%), micas (~1%), and a variable percentage of bioclasts. Estimated porosity in the sands varies from 10% to 35%.

At the top of the section (~380 m), sandstone-siltstone alternations pass upwards into a sand-rich facies (Figs. 12, 13D), which consists of moderately to well-sorted, very fine to fine/medium sands with silty layers. Bed thicknesses vary from 1 to 2 m (Fig. 12) and beds are locally composite or amalgamated. The dip-angle varies considerably with the lower and upper 15 m dipping at ~40º–45° towards the west, while the middle ~20 m have dips around 15° and are characterised by a higher content of silt and mud. In this sandy facies, the sand percentage is 70%–85%; the mud fraction varies between 12% and 28%.

4.3.1. Sedimentary structures

The base of the sand-rich facies (Fig. 12) shows a large incision that cuts into the underlying turbiditic succession (Fig. 15A). Locally it is possible to observe scours (Fig. 15B, C), covered by apparent cross-sets, which could also partly result from soft-sediment deformation (Fig. 15B). Rip-up mud clasts are abundant in the following forms: (i) mud-clast conglomerate (Fig. 15B, D); (ii) mud-clasts on toesets (Fig. 15D); and (iii) isolated floating clasts. Thinner beds (20–30 cm) show sharp lower and upper contacts, thin bioturbations (5

mm in diameter), upper divisions of bidirectional ripple cross-lamination, and lower divisions of mud-clasts (Fig. 15F). Silty marlstones are bioturbated and weathered throughout.

4.3.2. Age and palaeo-water depth estimation

The planktic foraminiferal assemblages are characterised by the high abundance of *G. miotumida*, whose FCO is at 7.25 Ma (Sierro, 1993; Hilgen et al., 2012). This marker species suggests an early Messinian age, while the presence of predominantly sinistral coiling neogloboquadrinids indicates that the section predates PF-Event 4 at 6.35 Ma (sinistral to dextral coiling change of *N. acostaensis*; e.g., Sierro, 1993; Krijgsman, 2004). The benthic foraminiferal assemblages contain species common in outer shelf and upper slope environments (*C. ungerianus, C. pachyderma, Cibicidoides dutemplei, S. bulloides, U. peregrina)*. Rare *C. kullenbergi* are present only in the lower part of the Haricha section. The percentage of upper slope taxa decreases and of shelf taxa increases upwards. The estimated environment of deposition is shelf-slope transition (150–250 m water depth), or slightly deeper (150–300 m water depth).

5. Interpretation of the facies associations in the South Rifian Corridor

We combined the interpretation of the facies and facies associations (Table 1) with the ranges of water depths

inferred from benthic foraminifera to discuss here the environmental meaning of each association.

5.1. Association F1: turbidites (Sidi Harazem and Haricha)

Facies association F1 occurs at Sidi Harazem and Haricha (Figs. 4, 12) and reflects sedimentation in a basinal turbidite system (*sensu* Mutti et al., 2003), dominated by gravity-driven currents flowing in the foredeep axial trough and on the outer limb of the growing orogenic wedge (Fig. 2). It is likely that at Sidi Harazem these currents flowed in the foredeep axial zone, E-W or ESE-WNW according to the orientation of the thrust front (Fig. 2), whereas at Haricha they were channelised on the orogenic wedge slope, in a relatively proximal sector that fed the more distal basinal turbidites of the axial foredeep (Gharb Basin) to the west (Figs. 1, 2).

At Sidi Harazem, the turbidites were deposited in a foredeep position, immediately to the south of the orogenic wedge thrust front (Fig. 2). In the regional context of an E–W axial foredeep (Figs. 1, 2), the paleocurrent trend of NNW–SSE (Fig. 4B) could indicate that the flow veered due to a local influence of topography on the turbiditic conduits (i.e., irregularities on the flexed substrate causing changes of current

direction), or that the flow was still channelised on the slope of one of the margins of the seaway.

At Haricha, sheeted turbidites occur in non-channelised lobes, suggesting that the turbidity current occurred in flat areas of the slope-apron system, possibly in a basin-filled complex (e.g., Mutti and Normark, 1987; Stow and Johansson, 2000). Small-scale, channelised features (Fig. 14C) above horizontally sheeted turbidites suggest that stronger turbidity currents could have bypassed the area leaving only the channels filled with sands. The dominant palaeocurrent pattern towards the NW derived from sole-marks (Fig. 14D) indicates the main direction of transport (Fig. 12), while minor trends towards the E–NE and S–SW could reflect the flow spreading radially across the slope fan.

At Haricha, facies association F1 passes upwards into the distinct facies association of deep-water massive sands (F1.1; Table 1). This association is dominated by sands (sand-shale ratio up to 8:1) and forms the upper ~50 m of sandstone interval 2 (Fig. 12). The principal depositional processes involved for this association are high-concentration turbidity currents and sandy debris flows (Stow and Johansson, 2000; Mutti et al., 2003; Haughton et al., 2009). Steepening of the tectonic slope may have triggered such mass flow events, as the emplacement of this lobe seems to have occurred in a channelised conduit (Fig. 15A). However, since the

underlying turbidites are extensive and tabular, it is likely that flow occurred in a trough-basin filled complex (Stow and Johannsson, 2000) and its occurrence may reflect a transition between basinal turbidite system (characterised by tabular fill) and the more restricted trough-conduit (expressed by the lobe-shaped base of the top ~50 m; Fig. 15A).

Both associations F1 and F1.1 show indications of bottom-current reworking of some sandstone beds (e.g., Stow and Lovell, 1979; Lovell and Stow, 1982; Shanmugam, 1993; Ito et al., 2002; Rebesco et al., 2014; Gong et al., 2016), such as: bidirectional ripple cross-lamination in the upper part of the beds, where the upper parallel-laminated sand and graded silt divisions are absent (Fig. 15F); bioturbation in the sand division along with mud-clasts (Fig. 15F); bioturbation in the sand divisions showing preferential orientation (Fig. 14E), which is up to 90° perpendicular (~N–S) with respect to the palaeocurrents inferred from the sole-marks (westward).

5.2. Association F2: blue marl (all units)

The blue marl facies association is present in all sections (Figs., 4, 7, 12) and represents a relatively low energy depositional environment, in which fine suspended sediments can be deposited.

Given the overall upper slope to basinal setting and water depths of 100–500 m, the three most likely depositional processes are: hemipelagic settling, bottom currents, and fine-grained turbidity currents. Those muds/marls associated with the turbidite-dominated facies associations are likely to include some portion of fine-grained turbidites, whereas the rest of the succession can be either hemipelagite or muddy contourite (Table 1).

Minimum sedimentation rates for parts of the blue marlstone sections, between the FCO *G. menardii* 5 and FCO *G. miotumida* (Fig. 4, located below 800 m and at 870 m, respectively), are 70 cm kyr^{-1}. Much higher sedimentation rates (163 cm/kyr^{-1}) are derived from the marlstone sections of the centre of the Saiss Basin (Barhoun and Bachiri Taoufiq, 2008) during the late Tortonian, between LCO *G. menardii 4* (7.51 Ma) and FCO *G. miotumida* (7.25 Ma). Such relatively high rates of sedimentation suggest that not all the blue marls are associated with hemipelagite deposition but could partly result from bottom-current transport, namely those associated with facies association F4.

5.3. Association F3: swaley cross-stratified sandstones (Ain Kansera)

Facies association F3 is found at Ain Kansera (Fig. 4) and allows us to reconstruct the location of the palaeo-

shoreline. It is usually found in storm-dominated sequences above fair-weather wave base (Leckie and Walker, 1982) or associated with river-dominated deltaic systems (Mutti et al., 2003; TInterri, 2011). At Ain Kansera, the lack of catastrophic river-flood products (e.g., gravels, pebbles, debrites; Mutti et al., 2003) suggests that the succession is more likely to be produced by the progradation of a linear clastic coast, in which swaley cross-stratification (SCS) would be found above hummocky cross-stratification (Leckie and Walker, 1982). Furthermore, the geometries of the sandstone intervals (Fig. 5F) in which SCS is found are similar to the Infralittoral Prograding Wedges (Hernández-Molina et al., 2000; Mitchell et al., 2012). We interpret F3 as indicative of a wave-dominated, infralittoral environment with variable sedimentary input from river mouths. This is consistent with the shelf-type benthic assemblage of the underlying marls (50-100 m water depth), and the sandstone intervals of Ain Kansera (Fig. 5F) probably represents a shallower (15-50 m water depth) infralittoral setting.

5.4. Association F4: sandy contourites (El Adergha, Ben Allou)

Facies Association F4 occurs in El Adergha and Ben Allou (Fig. 4, 12) and comprises: (1) unidirectional cross-bedded sandstone encased in upper-bathyal marlstones; (2) heterolithic facies with cross-bedding and wavy-

lamination; and (3) tabular muddy sandstone beds encased in marlstones and characterised by bi-gradational sequences.

5.4.1. Unidirectional cross-bedded sandstones – F4.1

The cross-bedded sandstones (Figs. 5D, 8) occur within mud-dominated successions that were deposited at water depths of 150–300 m based on benthic foraminifera. Abundant bioturbation and shell debris in the sands attest to a marine environment with adequate food supply, while the scale of cross-bedding suggests formation by subaqueous dunes. Subaqueous dunes of this scale (Table 2) require mean flow-velocities greater than 0.5–0.6 m s^{-1} (Flemming, 1992; Masson et al., 2004; Stow et al., 2009) which, at that depth, and in the absence of wave cross-bedding (HCS and SCS), were probably created by unidirectional bottom-currents funnelled in the deep seaway (e.g., Johnson and Baldwin, 1996; Anastas et al., 1997, 2006; Longhitano, 2013).

The compound (2nd order) cross-bedded sets are composed exclusively of downslope dipping cosets (1st order sets), and the absence of upslope-dipping sets may be indicative of unidirectional steady flow (Table 2).

The cross-stratified sands of El Adergha and Ben Allou are interpreted as relics of a dune field formed by west-directed, sandy-sheeted drifts on the northern

margin of the late Tortonian seaway. The dune field architecture and flow-dynamics are reflected in the stacking pattern of the cross-stratified successions. The lowermost cross-stratified succession at Ben Allou B is ~20 m thick and reflects the first preserved dune field migrating over the area (Figs. 7, 10B). The first set of this succession progrades over a horizontal surface (S0 in Fig. 10C) and the set thickness (Fig. 9C) appears to increase to the right (southwest), indicating that the upper bounding surface may preserve the original orientation of the stoss-side of the compound dune. Compound tabular sets of cross-bedding grading upward into trough cross-bedding (Fig. 10C) reflects increased flow velocity and bedform evolution with time (Middleton and Southard, 1984; Longhitano et al., 2014). Low angle cosets and thin cross-bedded sets could reflect the leeside, or bottomset, of larger dunes in a compound dune field (Dalrymple and Rhodes, 1995; Anastas et al., 1997). The clinoforms at Sidi Harazem or sandstone interval 2 of Ben Allou (Fig. 10E) may preserve the spatial and temporal evolution of a 'decaying dune-field', reflecting the local expansion and/or deceleration of flow (similar to the form-sets, *sensu* Anastas et al., 1997). However, lateral equivalents of these clinoforms in sandstone interval 2 are composed of simple cross-strata of medium thickness (Supplementary Fig. 2E), suggesting that flow was

steady in some parts of the dune field and waning in others.

5.4.2. Heterolithic facies (Ben Allou) – F4.2

The heterolithic sandstone–mudstone deposits are present at Ben Allou above and below the main sandstone intervals (Fig. 11). This facies appears to represent a lower-energy environment in which an alternation of sand and mud deposition can occur. The lack of extensive cross-stratification suggests that the main bottom current was weak and could not cause the substantial sand drift migration seen in the main sandstone intervals. However, intermittent tractive currents occurred, as suggested by wavy surfaces and small dunes (Fig. 11C-D), which give a radial palaeocurrent pattern (Fig. 7B).

Mud layers deposited between the sandstone beds reflect a drop in current velocity (carrying capacity) at that point. The lack of mud-drapes within the main cross-bedded sandstone intervals suggest that the current was steady and/or the water column had low suspended sediment concentration during dune field migration (Johnson and Baldwin, 1996; Dalrymple and James, 2010). According to Baas et al (2016), heterolithic facies in a mixed sandy-muddy flow are able to occur by increasing the amount of suspended cohesive sediment concentration, either during steady

flow or rapidly decelerating flow. This model provides a pragmatic alternative to sediments previously interpreted as the results of start–stop currents (Baas et al., 2016). On the other hand, the cross-sets of sandstone intervals 1 and 2 are essentially mud-free and occur within mud-dominated deposits (blue marls). Therefore, the heterolithic facies may represent the transition between periods of sand-drift migration (possibly with low suspended sediment concentration) and episodes of high suspended-sediment concentration and mud flocculation. This transition may be linked to varying flow velocity and/or higher and lower values of suspended-sediment concentration.

5.4.3. Sandstone–mudstone units with bi-gradational sequences – F4.3

At El Adergha (Fig. 4), the distinctive heterolithic deposits are less pronounced, and the transitional facies between mud- and sand-dominated facies associations (F1 and F2, respectively) is represented by sandstone-mudstone units with bi-gradational sequences (Fig. 5E). These units (Figs. 5E, 6E) show features similar to those of the classic contourite sequence (see Fig. 2 in Stow et al. 1998; Stow and Faugères, 2008).

This sequence of facies has been linked to long-term fluctuations of the current velocity (Hüneke and Stow; 2008; Stow and Faugères, 2008). At El Adergha, we infer

that the velocity of the current forming the contourite sequence of facies association F4.3 was lower than the velocity forming the cross-stratified sandstone intervals (F4.1). Preservation of cross-lamination in fossil contourites has long been a subject of debate, and the lack of lamination is thought to be a result of lower velocity currents and intense bioturbation (Shanmugam, 2006; Hüneke and Stow, 2008; Stow and Faugères, 2008; Rebesco et al., 2014). This close superposition of facies at El Adergha (F4.1 and F4.3) clearly indicates that the two may coexist in the same depositional environment and are likely to depend solely on flow velocity.

5.5. Seismic facies association

5.5.1. Elongated, separated mounded drift (Haricha)

The Haricha seismic profile (Fig. 16) extends from the structural high of Mount Bou Draa (Fig. 2) to the Gharb basin to the west for about 15 km. The two main post-orogenic seismic units are identified as continuous and high amplitude parallel reflections resting unconformably above the Rif nappe and the structural high. Both units are separated by a regional discontinuity and form an overall mounded shape, here interpreted as a mounded drift (Faugères et al., 1999, Nielsen et al., 2008, Rebesco et al., 2014).

The mounded drift is asymmetric, due to the lateral merging of the mound into the channel (moat) that lies next to the structural high. To the northwest, the mound has a more tabular seismic expression (2 in Fig. 16) and shows an upwardly-convex geometry. To the southeast, the mound has a steeper side identified by reflections migrating upslope (1 and channel migration arrow in Fig. 16). This upslope progradational trend is characterised by a change from long, continuous and sub-parallel reflections (aggradation phase) to short, less continuous and sigmoidal reflections (progradation phase). The progradation phase is marked by SE-downlapping reflections, with local chaotic, transparent and erosional features reflecting lateral migration of the channel axis.

The Messinian unit records the same moat (3 in Fig. 16) and mounded deposits (2, Fig. 16); however the system loses this character upwards where the drift is less channelised (4, Fig. 16). This change may reflect the evolution into a sheeted drift, formed by the interaction of the bottom current with a gentler relief at times when the bottom current was either less-focussed or migrated laterally due to the shallowing trend of the basin.

The geometry of the mounded drift (prograding eastward) suggests that it was generated by a bottom current flowing northward, forced against the eastern or north-

eastern margin of the Gharb Basin by Coriolis (Faugères et al., 1999; Llave et al., 2001).

Turbidity currents flowing into the basin may have been channelised towards the abyssal plain to the west (offshore Gharb Basin) and thus provided the fine-grained component that was reworked by bottom currents and redeposited in the mound to the NW. In the case of Haricha, the coast was probably orientated N–S or NW–SE (Fig. 1b). We can infer that the bottom-current was confined by a steep slope to the west into a channel orientated N–S to NE–SW. This trend is in line with the seismic evidence of a contourite channel formed by bottom currents directed approximately south to north to southwest to northeast at the exit of the Oued Beth area during the late Miocene (white arrow in Fig. 2; SCP/ERICO report, 1991).

6. DISCUSSION

6.1 Contourite drift in the seaway

In the western mouth of the South Rifian Corridor, distinct distributions of lithofacies associations permit reconstruction of four main, late Tortonian marine depositional environments (Fig. 17): (i) 0–100 m deep, infralittoral to shelf environments along the northern margin; (ii) 150–300 m deep, bottom current-dominated slope environments; (iii) 250–400 m deep axial foredeep; and (iv) the southern, passive margin, which is

characterised by marginal reefs in its marginal embayments (e.g., Gulf of Skoura; Charrière and Saint-Martin, 1989; Saint-Martin and Charrière, 1989; Fig. 1). This distribution suggests a foredeep depositional profile thickening towards the north against the thrust front consistent with seismic data across the Saiss Basin (Sani et al., 2007).

We propose that facies association F4 documents the sand-rich parts of a bottom-current transport path along the northern margin of the South Rifian Corridor (Figs. 17, 18). The upper bathyal benthic assemblage contained in the blue marlstones and the lack of wave cross-bedding in this facies association (F4) suggest that the sandy drift was formed in a deeper setting than the shelf. There are various possible interpretation of this facies (Table 1).

We considered a shelfal, purely tidal origin for this sandy drift. Sandwaves (large to very large dunes, *sensu* Ashley, 1990) and elongated sand ridges with superimposed smaller-scale bedforms are common on many continental shelves down to depths of ~150–200 m (Johnson and Baldwin, 1996). Wind-, storm-, or tide-dominated environments result in unidirectional or bidirectional bottom current pathways (Stride, 1982; Johnson and Baldwin, 1996; Dyer and Huntley, 1999; Daniell and Hughes, 2007). Tidal sand ridges typically show lateral accretion surfaces, and coarsening and

thickening upward trends as wave and current action is stronger near the crest (e.g., Belderson et al., 1982; Houbolt, 1982; Johnson and Baldwin, 1996). In the South Rifian Corridor examples, however, low-angle, lateral accretion surfaces (with respect to the sense of flow) are mostly absent in facies association F4, and the cross-sets are bounded by sub-horizontal, laterally extensive surfaces, indicating sheet-like cross-bedding rather than sand bars or sand ridges. The low-angle clinoforms observed at El Adergha (Fig. 5C) and Ben Allou (Fig. 10E) dip parallel to the reconstructed flow, and may therefore represent the morphology of a large dune ('formset', *sensu* Anastas et al., 1997) rather than lateral accretion surfaces. Discontinuity-bounded cosets (or foreset units) at Ben Allou (Fig. 9C) represent a depositional increment in the construction of the compound bed (Anastas et al., 1997). In estuarine settings, this depositional increment may form a tidal bundle, which is the result of the single tidal cycle (Visser, 1980). Large (0.5–5 m high) dunes in tidal-dominated estuarine settings usually migrate 25–75 m yr^{-1}, therefore 0.04–0.11 m per single (semi-diurnal) cycle (Dalrymple and Rhodes, 1995). In these compound beds, the lengths of the foreset units range between 0.5 to 2 m, therefore the amount of material deposited in one foreset unit and that removed to form each discontinuity surface appears to be far too large to be

the product of a single tidal cycle (Dalrymple and Rhodes, 1995; Anastas et al., 1997).

In seaways, tidal currents can be amplified by the strait constriction and result in predominantly unidirectional cross-bedding down to depths of 200-250 m (e.g., Santoro et al., 2002; Longhitano et al., 2012, 2014; Longhitano, 2013). The cross-bedded sandstones of facies association F4.1, however, do not show diagnostic features of tidal strait deposition such as cross-lamination bundles, bidirectional foresets, superposition of cross-strata with different transport direction in a vertical or lateral sequence, vertical evolution from 3D to 2D dunes, interfingering of mass flow conglomerates associated with the strait margin/centre (Surlyk and Noe-Nygaard, 1992; Mellere and Steel, 1996; Longhitano, 2013; Longhitano et al., 2014).

We infer that the muddy-sandy sediments were transported by fluctuating current velocities without apparent trend or cyclicity, and this feature, together with the consistency of palaeocurrent directions, are not consistent with the classic tidal strait facies tracts (Longhitano, 2013).

An alternative scenario to pure tidal-current forcing is the geostrophic current-dominated strait. A modern example is the exit of today's Strait of Gibraltar. Here,

two distinctly different sedimentary environments coexist (Fig. 1): the shelf offshore area around Cape Trafalgar, which reaches ~100 m water depth (Lobo et al., 2000, 2010) and the middle–upper slope to the west of Camarinal Sill (Fig. 1), located at depths between ~200 and 800 m (e.g., Nelson et al., 1993; Habgood et al., 2003; Hernández-Molina et al., 2006, 2014a). Near Cape Trafalgar, large, sandy dune fields are the products of mixed wind-, tide, and storm- driven processes, resulting in both symmetric and asymmetric bedforms.

West of the Camarinal Sill, the proximal domain of the contourite depositional system (Hernández-Molina et al., 2003, 2006) comprises depositional (e.g., dunes) and erosional features (e.g., channels) linked to Mediterranean overflow (Nelson et al., 1993; Hernández-Molina et al., 2003, 2014b). Large sandy dune fields (Hernández-Molina et al., 2016c; Ercilla et al., 2017) develop within the main channels and km-long furrows form on a middle–upper slope terrace at water depth of ~200-500 m, and both migrate west-northwest, along the Mediterranean outflow pathway (Hernández-Molina et al., 2014a; Supplementary Fig. 4).

Based on this present day analogue and the comparison of facies association F4 with the modern bedforms of the Gulf of Cadiz contourite system (Hernández-Molina et al., 2016c; Ercilla et al., 2017), we propose that the sandy drift in the South Rifian Corridor

is likely to be the ancient expression of Mediterranean overflow (Hernández-Molina et al., 2014a, b). In this highly segmented foreland basin (Fig. 18), tectonics and thus topography may have played a major role forcing the predominant bottom-current into narrow passages. Therefore, the dominant westerly progradation can also be formed by the overflow current superimposed on the tidal ebb, while antithetic palaeocurrent patterns may have been produced by up-channel tidal flood or eddies that modulated the unidirectional current, as occurs in the present-day Strait of Gibraltar (Boyum, 1967; Criado-Aldeanueva et al., 2006; Teles-Machado et al., 2007; García-Lafuente et al., 2011; Naranjo et al., 2015: Sammartino et al., 2015). In this interpretation, the sandy contourites (facies association F4) in the Rifian Corridor would represent the proximal sector of the Contourite Depositional System and the westward elongated, separated mounded drifts (Fig. 16) the distal sector of the same system (Hernández-Molina et al., 2003; Llave et al., 2007).

6.1.1. Sedimentary model for the superposition of sandy and muddy contourites

Mud-sand mixtures form sand patches and rippled sand sheets in areas and/or times of low current velocity along a sediment transport path (e.g., Belderson et al., 1982; Stow et al., 2009; Rebesco et al., 2014). The presence of blue marls, muddy-sandy beds with bi-

gradational sequences, and heterolithic facies above and below the cross-stratified successions (Figs. 4 and 7) indicates periods in which the rate of deposition of fine-grained sediment was higher because the unidirectional current was either weaker, or had migrated laterally.

We therefore suggest that part of the blue marls (facies association F2) represent muddy contourites associated with times or areas of lower velocity flow (Stow and Faugères, 2008; Rebesco et al., 2014). During times of vigorous bottom currents, the drift migrated downflow, and so did the dune fields leading to facies F4.1, whereas at times of weak bottom current the sedimentary system evolved vertically to lower-energy facies associations (F.4.2, F4.3; F2). When the bottom current was weak, secondary processes such as tidal currents or internal tides may also have become more influent on the depositional system (Shanmugam, 2006; Rebesco et al., 2014). In the Gulf of Cadiz contourite system, tides become the dominant process on the surface of channel-fills, or during periods of lateral (down- or up-slope) migration of the current (Stow et al., 2013; Hernández-Molina et al., 2016b).

6.2. Active tectonic structures controlling the Mediterranean overflow in the Rifian Corridor

The present-day Mediterranean overflow requires a density contrast between the two basins, and for this to

develop, a narrow neck-zone (i.e., sill) between the Mediterranean Sea and the Atlantic Ocean is required (Knutz, 2008; Legg et al., 2009). The Strait of Gibraltar, with its shallow, narrow topography has been the critical structure allowing the Plio-Quaternary Mediterranean overflow to form.

Tectonic and palaeogeographic constraints suggest which bathymetric highs potentially generated the overspill in the Rifian Corridor during the late Miocene. The Rif foreland basins were gradually uplifted and disconnectedfrom the late Tortonian onwards, influencing sedimentation patterns along the Rifian Corridor (e.g., Charrière and Saint-Martin; 1989; Capella et al., 2017). This tectonic phase contributed to post-orogenic deformation up to present-day (e.g., Chalouan et al., 2014). This process may have caused localised uplift of horsts forming narrow neck-zones (i.e., sills) which then allowed the formation of overspill geometries within the Rifian seaway.

At the Taza Sill, the point dividing the Guercif and Saiss depocentres (Fig. 18), uplift of structural highs occurred at the Tortonian/Messinian boundary and along both faults and folds related to the North Middle-Atlas fault system (e.g., Gomez et al., 2000; Chalouan et al., 2014). Furthermore, the cross-stratified sandstone intervals at Ben Allou show clear wedge-shaped geometries (Fig. 8B, E) and large channelised incisions

(Fig. 8C), above which soft sediment deformation is abundant (Fig. 9E). All this indicates an episode of syn-depositional generation of accommodation space that may have resulted from uplift on the Nzala des Oudayas fault, orientated NE-SW and perpendicular to the foredeep axis (Figs. 2, 17, 18; see Sani et al., 2007, for structure at depth). This fault is part of the Prerif Ridge system and is connected to the main thrusts to the south (Fig. 2). The position of the sandy cross-stratified deposits to the west of each of these anticlinal ridges that cross-cut the foredeep axis (Figs. 2, 17) and whose uplift postdates the orogenic wedge emplacement (Capella et al., 2017), suggests that it is at these bathymetric highs that hydraulic control was exerted on flow through the Rifian Corridor.

The late Tortonian age of the sandy contourite drift observed at Ben Allou and El Adergha could then reflect tectonic control on the Mediterranean overflow at the Taza Sill (Figs. 1, 17). Subsequently, unconformities marking the Tortonian/Messinian boundary in the Gharb (Roksandic and Soquip, 1990; SCP/ERICO report, 1991; Fig. 16) possibly indicate a later tectonic readjustment controlling the Rifian Corridor palaeogeography.

The effect of tectonic activity on margin sedimentation is particularly clear in the Gulf of Cadiz, where contouritic drift evolution was directly influenced by

tectonic pulses every 0.8-0.9 and 2.0-2.5 Myr since the latest Miocene (Hernández-Molina et al., 2014b; 2016a). The deformation of the complex Africa-Iberia plate-boundary appears to have continued up to present day (Chalouan et al., 2014; Gutscher et al., 2002; Koulali et al., 2011), well after the continental collision and emplacement of the Betic-Rif Arc in its current position at ca. 8 Ma (van Hinsbergen et al., 2014; Do Couto et al., 2016). It is therefore possible to infer a strong correlation between the post-collisional evolution of the Africa-Iberia plate boundary, the Mediterranean-Atlantic seaways and the sandy drifts.

7. Conclusions

Upper Tortonian mixed-clastic deposits at Ben Allou and El Adergha in northern Morocco show evidence of west-migrating bedforms produced in 150-400 m–deep seaway settings. This includes cross-bedding and sandstone-mudstone beds with bi-gradational sequences, produced by a westerly, unidirectional bottom current.

We interpret this current to be the result of Mediterranean overflow, possibly modulated by tides. Vertically superposed facies were once lateral equivalents along a bottom current transport path. Heterolithic facies represent the low-speed bedforms (sand patches and rippled sand sheets) along this path,

at times of decelerating or migrating current. Elongated, separated mounded drifts in seismic profiles suggest that the overflow continued throughout the early Messinian.

Tectonics is a major controlling factor in seaway contourite deposition, since it causes the restriction required for the overflow to form. The spatial distribution of the cross-bedded sandy drifts west of tectonic ridges that cross cut the seaway suggests that the coeval uplift of these structures formed the highs required to generate Mediterranean overflow.

Acknowledgements

This work was funded by the People Programme of the European Union's 7th Framework Programme FP7/2007-2013/ under REA Grant Agreement No. 290201 (MEDGATE); F.J.H-M. wishes to acknowledge the CTM2012-38248, SA263U14 and CTM 2012-39599-C03 Projects; the "Drifters" Research Group of the Royal Holloway University of London (UK). We thank ONHYM for providing unpublished datasets and field support; Estefanía Llave (IGME, Spain), M. Amine Manar (ONHYM, Morocco), Paul Meijer (UU, The Netherland), Francois Raisson (TOTAL, France), and Antoine Thieblemont (RHUL, UK) for their assistance during fieldwork and for stimulating discussions. Journal reviews by Ed. Jasper Knight and two anonymous

reviewers are greatly appreciated, and their comments helped us to improve the clarity of the manuscript.

Appendix A. Supplementary figures.

Supplementary figures to this article can be found online at http://

Figure captions

Fig. 1. (A) Generalised tectonic map of the Betic-Rif arc with location of the study area (Fig. 2) and distribution of the Mediterranean Overflow Water. Structural units modified after Vergés and Fernandez (2012). AT: Arbaa Taourirt; CS: Camarinal Sill; CT: Cape Trafalgar; GhB: Gharb Basin; GS: Gibraltar Straits; GuB: Guadalquivir Basin; IB: Intramontane Basins; NMAF: North-Middle-Atlas Fault; SB: Saiss Basin; Sk: Gulf of Skoura; TGB: Taza-Guercif Basin; TS: Taza Sill. 1: thrust; 2: normal fault; 3: strike-slip; 4: faults; 5: buried thrust. (B) Approximate palaeogeography of the Betic and Rifian Corridor during the late Miocene modified after Flecker et al. (2015). White dotted lines are the present-day coastline. Location of the studied section in the palaeogeographic context: BA= Ben Allou; EF= East Fes; HA = Haricha.

Fig. 2. (A) Stratigraphic column and tectonogram illustrating the relationship between lithostratigraphy and tectonic in the Rif foreland (after Capella et al., 2017). (B) Geological map of the study area with location

of the sections (East Fes, Ben Allou, and Haricha) and seismic profile shown in Fig. 16. Tectonic lineaments in the Saiss, eastern Gharb basin, and the southern margin of the external Rif thrust-sheets are compiled after Sani et al. (2007); Capella et al. (2017). The extent of upper Tortonian – Messinian units is modified after the results of the present study.

Fig. 3. Correlation diagram between the studied sections and the classic Gharb-Saiss stratigraphy. The 5 studied sections (Sidi Harazem, El Adergha, Ain Kansera, Ben Allou, and Haricha) are dated with biostratigraphy. Bioevents (left column): Sx= Onset dominant sinistral; FO= First occurrence; LCO= Last common occurrence; FCO= First common occurrence; S/D= coiling change from predominantly sinistral to dextral (after Lourens et al., 2004; Hilgen et al., 2012). Dotted fills depict the sand-rich parts, whereas simple colour fill broadly represents other lithologies (e.g., marlstone, limestone).

Fig. 4. (A) Stratigraphic logs of Sidi Harazem, El Adergha and Ain Kansera units with brief lithological description and age determination based on planktonic foraminifera (see text for further details). Detailed sedimentary log of the upper part of El Adergha shows the stacking pattern of the cross-stratified sand beds. Location of the sites on Fig. 5A. (B) Palaeocurrents from the three units showing number (n) of data per each site.

Fig. 5. (A) Satellite image of the East Fes section, showing the location of the Sidi Harazem, El Adergha, Ain Kansera units, and of pictures B, C, and F (adapted from Google Earth). (B) Outcrop of the Sidi Harazem section, showing the typical sandstone-marlstone alternation. (C) View of the El Adergha section. (D) Close view of the upper El Adergha section, showing the geometry of the upper bedset with prograding clinoforms. (E) Example of one of the sandstone–mudstone beds with bi-gradational sequences from El Adergha, interpreted as contourites. (F) Outcrop view of the Ain Kansera section, showing laterally extensive sandstone intervals at the top.

Fig. 6. (A) Close-up of the Sidi Harazem sand-marl alternation, interpreted as sandy turbidites. Bioturbation is interpreted as Zoophycus (left) and Chondrites (right). (B) A sludge-mark at the base of a turbidite bed at Sidi Harazem is filled with a ~5 cm thick cross-laminated sandstone division. (C) 2D cross-sets at El Adergha are mostly unidirectional and up to ~50 cm in thickness. White dotted lines depict surfaces of the clinoforms drawn in Fig. 5D. (D) Small set of cross-bedding and ripple laminations. (E) Close-up observation of a sandy contourite at El Adergha (location in outcrop in Fig. 5D) showing bi–gradational sequences analogous to the contourite facies model of Stow et al. (1998) and Stow and Faugères (2008). (F, G) Examples of the

swaley-cross stratification found in the Ain Kansera sandstone intervals.

Fig. 7. (A) Stratigraphic and sedimentary logs of Ben Allou section. Ben Allou B is a representative stratigraphic log of the Ben Allou section, with the zoom-in to the left showing the sedimentary log of sandstone interval 1a and 1b. Ben Allou A shows the detailed sedimentary log of the laterally equivalent sequence in the north-east site (location in Fig. 8A). (B) Palaeocurrent pattern of Ben Allou section from 2D and 3D cross-sets (left) and small cross-sets in heterolithic facies (right).

Fig. 8. (A) Oblique satellite image of the Ben Allou section with location of the logging paths (Ben Allou A and B), linear trend of the sandstone interval 1 and 2, and pictures B, C and E. (B) Outcrop view of Ben Allou A section. There is a discordance (angular unconformity) between SU1a and SU1b. The marlstones between the two units are wedging out towards the northeast. (C) Sandstone interval 1a at Ben Allou B showing the lateral continuity of the cross-sets, and channel-form displaying an ENE-WSW axis, a width of around 50m and incision depth of 15m. (D) Side-view of the same channel-form of Fig. 8C with view to the north-east. (E) Panoramic view of the discordance between sandstone intervals 1 and 2 at Ben Allou B. The two intervals bend in a gentle synform.

Fig. 9. (A) Relationship between different order cross-stratification at Ben Allou. First-order sets are small dunes prograding down the lee-side of larger dunes (2nd order sets). (B) West-migrating, medium thickness, simple cross-bedding with tabular geometry at Ben Allou A, SI-1a. (C) West-migrating, medium to large, compound cross-bedding at Ben Allou B, SI-1a. (D) Well-preserved dune over-riding a larger dune. (E) Fluid-escape structures occur in cross-sets and are capped by undeformed set-boundaries. (F) Planolites burrowing the surface of a foreset.

Fig. 10. (A-B) Photomosaic showing the lowermost cross-stratified succession at Ben Allou B, truncated by the channel-form of Fig. 8C at the top. The first set on the right corresponds to Fig. 9C. The black arrow indicates the same bed. (C) Line drawing of the combined pictures A-B. (D) Photomosaic of a cross-stratified succession in SI-2. For location see Fig. 8E. (E) Line-drawing of (D) with emphasis on the discontinuities between sets.

Fig. 11. (A) Heterolithic beds composed of cm- to dm-thick sandstone intervals and mm- to cm-thick mudstone layers. (B) Wavy bounding surface between mudstone layers and sandstone beds. In the top right corner, indistinct cross-laminations are visible. (C) Small cross-sets are preserved in some of the sandstone beds. Note the mudstone draping the bedform geometry. (D)

Wavy lamination formed by thin alternations of mudstone and sandstone.

Fig. 12. Stratigraphic log of the Haricha section, with detailed sedimentary log of the top ~50 m, sand-rich facies. Plotted palaeocurrent data corresponding to sole-marks in the sand-marl alternations.

Fig. 13. (A) Oblique satellite image with location of the main lithological units at Mount Haricha. The section is tilted and the layers plunge into the Gharb Basin to the west. Note the view towards the southwest. (B) Panoramic picture showing the contact between the lower part of the section and the Rif nappe of the orogenic wedge. (C) Panoramic picture of the sand-marl alternation of the upper part of the section (white dotted lines are drawn above prominent sand beds). This alternation grades upwards into the sand-rich facies (D). (E) Close-up of the onset of the amalgamated sandstone beds making the top ~50 m of the Haricha section.

Fig. 14. Close-ups on turbidite features at Haricha. (A) Purple-coloured sandstone bed from the lower part, with a basal division of cross-lamination. Note the bioturbation throughout. (B) Bioturbation on the top of the same sandstone beds, interpreted as Rhyzocorallium. (C) Photomosaic of a road cut showing tabular sandstone beds and sandstone with scour-and-fill features. The sandstone beds are encased in silty

marlstones. (D) Sole-marks (groove-casts) in a bioturbated base. (E) Example of a sandbed with superposition of divisions of massive sand (base) and parallel-laminated sand. Preferential orientation of bioturbation-like features is shown.

Fig. 15. Details of Haricha-top sand-rich facies, interpreted as deep-water massive sands. (A) Outcrop view of the base of the ~50 m thick, sand-rich facies. White dotted lines depict the bedding attitude of the underlying turbidite beds. (B) Close-up of the mud-clast conglomerate forming scours and diffuse (or deformed) stratification in the amalgamated beds. (C) Scours in coarser layer. (D) Rip-up mud clasts occur between massive sand (below) and cross-laminated sand (above). (E) Example of chaotic mud clast conglomerate. (F) Close-up of a thin (20 cm thick) sandstone bed encased in ungraded siltstone.

Fig. 16. ONHYM (Office National des Hydrocarbures et des Mines) multichannel seismic line (below) crossing Haricha section and prolongation of structures to the surface (above). Profile location in Fig. 2. The profile shows the Tortono-Messinian, post-orogenic (post-nappe) seismo-stratigraphic units with an elongated, separated mounded drift. Seismic facies: (2) continuous and sub-parallel reflections; (1) discontinuous, sigmoidal, and downlapping reflections; (3) channel or moat; (Blue arrow) channel migration.

Fig. 17. Interpretative sketch with sedimentary environments and bedform distribution in a deep, foreland-basin seaway. This genetic model relates to a conceptual distribution of bedforms under dominantly unidirectional current and explains the mixed environments observed in the South Rifian Corridor. BCRS = Bottom Current Reworked Sands.

Fig. 18. Palaeogeographic map of the Rifian Corridor at the Tortonian-Messinian boundary. Active tectonic structures after Sani et al., 2007; Chalouan et al., 2014; Capella et al., 2017. NF: Nekor Fault; JF: Jebha Fault; NMF: North Middle-Atlas Fault. GhB: Gharb Basin; SB: Saiss Basin; TGB: Taza-Guercif Basin. Sections indicated with a white star are: El Adergha (1), Ben Allou (2). Yellow star depicts the position of the drift inferred from seismic data in the Gharb Basin (Fig. 16).

Table 1. Summary of lithofacies and possible genetic mechanisms.

Table 2. Levels and varieties of cross-stratification present in facies association F4.1 (unidirectional cross-bedded sandstones). Mechanisms of formation after Anastas et al., 1997.

References

Achalhi, M., Münch, P., Cornée, J.J., Azdimousa, A., Melinte-Dobrinescu, M., Quillévéré, F., Drinia, H., Fauquette, S., Jiménez-Moreno, G., Merzeraud,

G., Moussa, A.B., El Karim, Y., Feddi, N., 2016. The late Miocene Mediterranean-Atlantic connections through the North Rifian Corridor: New insights from the Boudinar and Arbaa Taourirt basins (northeastern Rif, Morocco). Palaeogeography, Palaeoclimatology, Palaeoecology 459,131-152.

Anastas, A.S., Dalrymple, R.W., James, N.P., Nelson, C.S., 1997. Cross-bedded calcarenites from New Zealand: subaqueous dunes in a cool-water Oligo-Miocene seaway. Sedimentology 44, 869- 891.

Anastas, A.S., Dalrymple, R.W., James, N.P., Nelson, C.S., 2006. Lithofacies and dynamics of a cool-water carbonate seaway: Mid-Tertiary, Te Kuiti Group, New Zealand. Geological Society, London, Special Publication 255, 245-268.

Anovitz, L.M., Cole, D.R., 2015. Characterization and analysis of porosity and pore structures. Reviews in Mineralogy and geochemistry 80, 61-164.

Ashley, G.M., 1990. Classification of large-scale subaqueous bedforms: a new look at an old problem-SEPM bedforms and bedding structures. Journal of Sedimentary Research 60.

Baas, J.H., Best, J.L., Peakall, J., 2016. Predicting bedforms and primary current stratification in cohesive mixtures of mud and sand. Journal of the Geological Society 173, 12-45.

Barbero, L., Jabaloy, A., Gómez-Ortiz, D., Pérez-Peña, J.V., Rodríguez-Peces, M.J., Tejero, R., Estupiñán, J., Azdimousa, A., Vázquez, M., Asebriy, L., 2011. Evidence for surface uplift of the Atlas Mountains and the surrounding peripheral plateaux: Combining apatite fission-track results and geomorphic indicators in the Western Moroccan Meseta (coastal Variscan Palaeozoic basement). Tectonophysics 502, 90-104.

Barhoun, N., Bachiri Taoufiq, N., 2008. Événements biostratigraphiques et environnementaux enregistrés dans le corridor sud rifain (Maroc septentrional) au Miocène supérieur avant la crise de salinité messinienne. Geodiversitas 1, 21-40.

Belderson, R.H., Johnson, M.A., Kenyon, N.H., 1982. Bedforms. In: Stride, A.H. (Ed.), Offshore Tidal Sands: Processes and Deposits. Chapman & Hall, London, pp. 27-57.

Benson, R.H., Bied, R.E., Bonaduce, G., 1991. An important current reversal (influx) in the Rifian Corridor (Morocco) at the Tortonian-Messinian boundary: The end of Tethys Ocean. Palaeoceanography 6, 165-192.

Boyum, G., 1967. Hydrological observations of the M/S “Helland-Hansen” and current measurements in the area west of Gibraltar. NATO Sub-Committee

on Oceanographic Research Technical Reports 34, 35–36.

Capella, W., Matenco, L., Dmitrieva, E., Roest, W.M., Hessels, S., Hssain, M., Chakor-Alami, A., Sierro, F.J., Krijgsman, W., 2017. Thick-skinned tectonics closing the Rifian corridor. Tectonophysics. doi:10.1016/j.tecto.2016.09.028.

Caralp, M.H., 1984. Quaternary calcareous benthic foraminifers. Initial Reports of the Deep Sea Drilling Project 80, 725-755.

Chalouan, A., Michard, A., El Kadiri, K., Negro, F., de Lamotte, D.F., Soto, J.I., Saddiqi, O., 2008. The Rif Belt. In: Michard, A., Saddiqi, O., Chalouan, A., Frizon de Lamotte, D. (Eds.), Continental evolution: the geology of Morocco. Springer, Berlin-Heidelberg, pp. 203-302.

Chalouan, A., Gil, A.J., Galindo-Zaldívar, J., Ruano, P., de Lacy, M.C., Ruiz-Armenteros, A.M., Benmakhlouf, M., Riguzzi, F., 2014. Active faulting in the frontal Rif Cordillera (Fes region, Morocco): Constraints from GPS data. Journal of Geodynamics 77, 110-122.

Charrière, A., Saint-Martin, J.P., 1989. Relations entre les formations récifales du Miocène supérieur et la dynamique d'ouverture et de fermeture des communications marines à la bordure

méridionale du sillon sud-rifain (Maroc). Comptes Rendus de l'Académie des Sciences II 309, 611-614.

Cirac, P., 1987. Le bassin sud-rifain occidental au Néogène supérieur. Mémoires de l'Institut de Géologie du Bassin d'Aquitaine 21.

Crampton, S.L., Allen, P.A., 1995. Recognition of forebulge unconformities associated with early stage foreland basin development: example from the North Alpine Foreland Basin. AAPG bulletin 79, 1495-1514.

Criado-Aldeanueva, F., García-Lafuente, J., Vargas, J.M., Del Río, J., Vázquez, A., Reul, A.. Sánchez, A., 2006. Distribution and circulation of water masses in the Gulf of Cadiz from in situ observations. Deep Sea Research Part II: Topical Studies in Oceanography 53, 1144-1160.

Dalrymple, R., 1984. The morphology and internal structure of sandwaves in the Bay of Fundy. Sedimentology 31, 365-382.

Dalrymple, R.W., Rhodes, R.N., 1995. Estuarine dunes and bars.Developments in sedimentology 53, 359-422.

Dalrymple, R.W. , James, N.P. (Eds.), 2010. Facies Models 4. Geological Association of Canada, Calgary, AB.

Daniell, J.J., Hughes, M., 2007. The morphology of barchan-shaped sand banks from western Torres Strait, northern Australia. Sedimentary Geology 202, 638-652.

Dayja, D., 2002. Les foraminifères néogènes, témoins de la chronologie, de la bathymétrie et de l'hydrologie du Corridor Rifain (Maroc septentrional). Doctoral dissertation, Paris 6.

Dayja, D., Janin, M.C., Boutakiout, M., 2005. Biochronologie et corrélation des bassins néogènes du Couloir sud-rifain (Maroc) fondées sur les évènements de foraminifères planctoniques et de nannofossiles calcaires. Revue de micropaléontologie 48, 141-157.

de la Vara, A., Topper, R.P., Meijer, P.T., Kouwenhoven, T.J., 2015. Water exchange through the Betic and Rifian corridors prior to the Messinian Salinity Crisis: A model study. Paleoceanography 30), 548-557.

Do Couto, D., Gorini, C., Jolivet, L., Lebret, N., Augier, R., Gumiaux, C., d'Acremont, E., Ammar, A., Jabour, H. , Auxietre, J.L., 2016. Tectonic and stratigraphic evolution of the Western Alboran Sea Basin in the last 25 Myrs. Tectonophysics 677, 280-311.

Dorst, S., Schönfeld, J., 2013. Diversity of benthic foraminifera on the shelf and slope of the NE Atlantic: Analysis of datasets. Journal of Foraminiferal Research 43, 238-254.

Duggen, S., Hoernle, K., Van Den Bogaard, P., Rüpke, L., Morgan, J.P., 2003. Deep roots of the Messinian salinity crisis. Nature 422(6932), 602-606.

Dumas, S., Arnott, R.W.C., 2006. Origin of hummocky and swaley cross-stratification—The controlling influence of unidirectional current strength and aggradation rate. Geology 34, 1073–1076.

Dyer, K.R., Huntley, D.A., 1999. The origin, classification and modelling of sand banks and ridges. Continental Shelf Research 19, 1285-1330.

Ercilla, G., Casas, D., Hernández-Molina, F.J., Roque, C., 2017. Generation of Bedforms by the Mediterranean Outflow Current at the Exit of the Strait of Gibraltar, in: Guillén, J., Acosta, J., Chiocci, F.L., Palanques, A. (Eds.), Atlas of Bedforms in the Western Mediterranean. Springer International Publishing, Cham, pp. 273–280. doi:10.1007/978-3-319-33940-5_42

Faugères, J.C., Stow, D.A., Imbert, P. and Viana, A., 1999. Seismic features diagnostic of contourite drifts. Marine Geology, 162(1), 1-38.

Feinberg, H., 1986. Les séries tertiaires des zones externes du Rif (Maroc); biostratigraphie, paléogéographie et aperçu tectonique. Notes et Mémoires du Service Géologique du Maroc 315, 192.

Flecker, R., Krijgsman, W., Capella, W., de Castro Martíns, C., Dmitrieva, E., Mayser, J.P., Marzocchi, A., Modestou, S., Ochoa, D., Simon, D., Tulbure, M., van den Berg, B., van der Schee, M., de Lange, G., Ellam, R., Govers, R., Gutjahr, M., Hilgen, F., Kouwenhoven, T., Lofi, J., Meijer, P., Sierro, F.J., Bachiri, N., Barhoun, N., Alami, A.C., Chacon, B., Flores, J.A., Gregory, J., Howard, J., Lunt, D., Ochoa, M., Pancost, R., Vincent, S., Yousfi, M.Z., 2015. Evolution of the Late Miocene Mediterranean–Atlantic gateways and their impact on regional and global environmental change. Earth-Science Reviews 150, 365-392.

Flemming, B.W., 1992. Bed phases in bioclastic sands exposed to unsteady, non-equilibrated flows: an experimental flume study. Senckenbergiana Maritima 22, 95-108.

Fontanier, C., Jorissen, F.J., Licari, L., Alexandre, A., Anschutz, P., Carbonel, P., 2002. Live benthic foraminiferal faunas from the Bay of Biscay: faunal density, composition, and microhabitats. Deep-Sea Research Part I : Oceanographic Research Papers 49, 751-785.

Frizon de Lamotte, D., 1979. Contribution à l'étude de l'évolution structural du Rif oriental (Maroc). Doctoral dissertation, Paris 6.

García-Lafuente, J., Sánchez-Román, A., Naranjo, C., Sánchez-Garrido, J.C., 2011. The very first transformation of the Mediterranean outflow in the Strait of Gibraltar. Journal of Geophysical Research 116, C07010.

Gelati, R., Moratti, G., Papani, G., 2000. The Late Cenozoic sedimentary succession of the Taza-Guercif Basin, South Rifian Corridor, Morocco. Marine and Petroleum Geology 17, 373-390.

Gomez, F., Barazangi, M., Demnati, A., 2000. Structure and evolution of the Neogene Guercif Basin at the junction of the Middle Atlas Mountains and the Rif Thrust Belt, Morocco. AAPG bulletin 84, 1340-1364.

Gong, C., Wang, Y., Zheng, R., Hernández-Molina, F.J., Li, Y., Stow, D., Xu, Q., Brackenridge, R.E., 2016. Middle Miocene reworked turbidites in the Baiyun Sag of the Pearl River Mouth Basin, northern

South China Sea margin: Processes, genesis, and implications. Journal of Asian Earth Sciences 128, 116-129.

Gutscher, M.A., Malod, J., Rehault, J.P., Contrucci, I., Klingelhoefer, F., Mendes-Victor, L., Spakman, W., 2002. Evidence for active subduction beneath Gibraltar. Geology 30, 1071-1074.

Habgood, E.L., Kenyon, N.H., Masson, D.G., Akhmetzhanov, A., Weaver, P.P., Gardner, J., Mulder, T., 2003. Deep-water sediment wave fields, bottom current sand channels and gravity flow channel-lobe systems: Gulf of Cadiz, NE Atlantic. Sedimentology 50, 483-510.

Hardage, B.A. 1987. Seismic Stratigraphy. Geophysical Press Ltd, ISBN 0-946631-09-3.

Haughton, P., Davis, C., McCaffrey, W., Barker, S., 2009. Hybrid sediment gravity flow deposits–classification, origin and significance. Marine and Petroleum Geology 26, 1900-1918.

Hernández-Molina, F.J., Fernández-Salas, L.M., Lobo, F., Somoza, L., Díaz-del-Río, V., Alveirinho Dias, J.M., 2000. The infralittoral prograding wedge: a new large-scale progradational sedimentary body in shallow marine environments. Geo-Marine Letters 20, 109–117.

Hernández-Molina, F.J., Llave, E., Somoza, L., Fernández-Puga, M.C., Maestro, A., León, R.,

Medialdea, T., Barnolas, A., García, M., Díaz del Río, V., Fernández-Salas, L.M., Vázquez, J.T., Lobo, F., Alveirinho Dias, J.M., Rodero, J., Gardner, J., 2003. Looking for clues to palaeoceanographic imprints: a diagnosis of the Gulf of Cadiz contourite depositional systems. Geology 31, 19-22.

Hernández-Molina, F.J., Llave, E., Stow, D.A.V., García, M., Somoza, L., Vázquez, J.T., Lobo, F.J., Maestro, A., del Río, V.D., León, R., Medialdea, T., 2006. The contourite depositional system of the Gulf of Cadiz: a sedimentary model related to the bottom current activity of the Mediterranean outflow water and its interaction with the continental margin. Deep Sea Research Part II: Topical Studies in Oceanography 53, 1420-1463.

Hernández-Molina, F.J., Paterlini, M., Violante, R., Marshall, P., de Isasi, M., Somoza, L., Rebesco, M., 2009. Contourite depositional system on the Argentine slope: an exceptional record of the influence of Antarctic water masses. Geology 37, 507–510.

Hernández-Molina, F.J., Serra, N., Stow, D.A.V., Llave, E., Ercilla, G., Van Rooij, D., 2011a. Along-slope oceanographic processes and sedimentary products around the Iberian margin. Geo-Marine Letters 31, 315–341.

Hernández-Molina, F.J., Llave, E., Preu, B., Ercilla, G., Fontan, A., Bruno, M., Serra, N., Gomiz, J.J., Brackenridge, R.E., Sierro, F.J., Stow, D.A., 2014a. Contourite processes associated with the Mediterranean Outflow Water after its exit from the Strait of Gibraltar: Global and conceptual implications. Geology 42, 227-230.

Hernández-Molina, F.J., Stow, D.A.V., Alvarez-Zarikian, C.A., Acton, G., Bahr, A., Balestra, B., Ducassou, E., Flood, R., Flores, J.A., Furota, S., Grunert, P., Hodell, D., Jimenez-Espejo, F., Kim, J.K., Krissek, L., Kuroda, J., Li, B., Llave, E., Lofi, J., Lourens, L., Miller, M., Nanayama, F., Nishida, N., Richter, C., Roque, C., Pereira, H., Sanchez Goñi, M.F., Sierro, F.J., Singh, A.D., Sloss, C., Takashimizu, Y., Tzanova, A., Voelker, A., Williams, T., Xuan, C., 2014b. Onset of Mediterranean outflow into the North Atlantic. Science 344 (6189), 1244-1250.

Hernández-Molina, F.J., Llave, E., Sierro, F.J., Roque, C., Van der Schee, M., Williams, T., Ledesma, S., Arnais, A., Rosales, C., Brackenridge, R.E., Stow, D.A.V., 2016a. Evolution of the Gulf of Cadiz Margin and west Portugal contourite depositional system: tectonic, sedimentary and paleoceanographic implications from IODP Expedition 339. Marine Geology 377, 7-39.

Hernández-Molina, F.J., Wåhlin, A., Bruno, M., Ercilla, G., Llave, E., Serra, N., Roson, G., Puig, P., Rebesco, M., Van Rooij, D., Roque, C., González-Pola, C., Sánchez, F., Gómez, M., Preu, B., Schwenk, T., Hanebuth, Till J.J., Sánchez Leal, Till J.J., García-Lafuente, J., Brackenridge, Rachel E., Juan, C., Stow, Dorrik A.V., Sánchez-González, J.M., 2016b. Oceanographic processes and products around the Iberian margin: a new multidisciplinary approach. Marine Geology 378, 127-156.

Hernández-Molina, F.J.; Ercilla, G., Casas, D., Roque, C., Stow, D.A.V., MOWER Cruise team, 2016c. Larger morphological sea-floor features and bedforms associated to the Mediterranean Outflow Water in the Gulf of Cadiz. In: Van Landeghem, K.J.J., Garlan T., Baas, J.H. (Eds), MARID 2016. Fifth International Conference on Marine and River Dune Dynamics, Caernarfon, United Kingdom, 4–6 April 2016. Bangor University and SHOM, Abstract volume, 216 pp. ISBN 978-2-11-128417-3.

Hilgen, F.J., Krijgsman, W., Langereis, C.G., Lourens, L.J., Santarelli, A., Zachariasse, W.J., 1995. Extending the astronomical (Polarity) time scale into the Miocene. Earth and Planetary Science Letters 136, 495-510.

Hilgen, F.J., Bissoli, L., Iaccarino, S., Krijgsman, W., Meijer, R., Negri, A., Villa, G., 2000. Integrated stratigraphy and astrochronology of the Messinian GSSP at Oued Akrech (Atlantic Morocco). Earth and Planetary Science Letters 182, 237-251.

Hilgen, F.J, Lourens, L.J., Van Dam, J.A., 2012. The Neogene Period. In: Gradstein, F.M., Ogg, J.G., Schmitz, M., Ogg, G. (Eds.), The geologic time scale, Elsevier, Boston, pp. 923-978.

Hinsbergen, D.J., Vissers, R.L., Spakman, W., 2014. Origin and consequences of western Mediterranean subduction, rollback, and slab segmentation. Tectonics 33, 393-419.

Hohenegger, J., 2005. Estimation of environmental paleogradient values based on presence/absence data: a case study using benthic foraminifera for paleodepth estimation. Palaeogeography, Palaeoclimatology, Palaeoecology 217, 115-130.

Houbolt, J.J.H.C., 1982. A comparison of recent shallow marine tidal sand ridges with Miocene sand ridges in Belgium. The ocean floor, Chichester, John Wiley, pp.69-80.

Hüneke, H., Stow, D.A.V., 2008. Identification of ancient contourites: problems and palaeoceanographic significance. Developments in Sedimentology 60, 323-344.

Hüneke, H, Henrich, R., 2011. Pelagic sedimentation in modern and ancient oceans. In: Hüneke, H., Mulder, T. (Eds.), Deep-sea sediments. Elsevier, Amsterdam, The Netherlands, pp. 215-351.

Iribarren, L., Vergés, J., Fernández, M., 2009. Sediment supply from the Betic–Rif orogen to basins through Neogene. Tectonophysics 475, 68-84.

Ito, M., 2002. Kuroshio current-influenced sandy contourites from the Plio-Pleistocene Kazusa forearc basin, Boso Peninsula, Japan. Geological Society, London, Memoirs 22, 421-432.

Ivanovic, R.F., Flecker, R., Gutjahr, M.,Valdes, P.J., 2013. First Nd isotope record of Mediterranean–Atlantic water exchange through the Moroccan Rifian Corridor during the Messinian salinity crisis. Earth and Planetary Science Letters 368, 163-174.

Johansson, M., Stow, D.A. V, 1995. A classification scheme for shale clasts in deep water sandstones. Geological Society, London, Special Publication 94, 221–241.

Johnson, H.D., Baldwin, C.T. Shallow clastic seas. In: Reading, H.(Ed.), Sedimentary environments: processes, facies and stratigraphy 3rd ed., Wiley-Blackwell, 1996, pp.232-280.

Jorissen, F.J., de Stigter, H.C., Widmark, J.G.V., 1995. A conceptual model explaining benthic

foraminiferal microhabitats. Marine Micropaleontology 26, 3-15.

Knutz, P.C., 2008. Palaeoceanographic significance of contourite drifts.Developments in Sedimentology 60, 511-535.

Koulali, A., Ouazar, D., Tahayt, A., King, R.W., Vernant, P., Reilinger, R.E., McClusky, S., Mourabit, T., Davila, J.M., Amraoui, N., 2011. New GPS constraints on active deformation along the Africa–Iberia plate boundary. Earth and Planetary Science Letters 308, 211-217.

Krijgsman, W., Hilgen, F.J., Langereis, C.G., Santarelli, A., Zachariasse, W.J., 1995. Late Miocene magnetostratigraphy, biostratigraphy and cyclostratigraphy in the Mediterranean. Earth and Planetary Science Letters 136, 475-494.

Krijgsman, W., Langereis, C.G., Zachariasse, W.J., Boccaletti, M., Moratti, G., Gelati, R., Iaccarino, S., Papani, G.,Villa, G., 1999. Late Neogene evolution of the Taza–Guercif Basin (Rifian Corridor, Morocco) and implications for the Messinian salinity crisis. Marine Geology 153, 147-160.

Krijgsman, W., Gaboardi, S., Hilgen, F.J., Iaccarino, S., Kaenel, E.D., van der Laan, E.., 2004. Revised astrochronology for the Ain el Beida section (Atlantic Morocco): no glacio-eustatic control for

the onset of the Messinian Salinity Crisis. Stratigraphy 1, 87-101.

Leckie, D.A., Walker, R.G., 1982. Storm-and tide-dominated shorelines in Cretaceous Moosebar-Lower Gates interval--outcrop equivalents of Deep Basin gas trap in western Canada. AAPG Bulletin 66, 138-157.

Legg, S., Ezer, T., Jackson, L., Briegleb, B.P., Danabasoglu, G., Large, W.G., Wu, W., Chang, Y., Ozgokmen, T.M., Peters, H., Xu, X., 2009. Improving oceanic overflow representation in climate models: the gravity current entrainment climate process team. Bulletin of the American Meteorological Society 90, 657-670.

Lin, W., Tadai, O., Takahashi, M., Sato, D., Hirose, T., Tanikawa, W., Hamada, Y., Hatakeda, K., 2015. An Experimental Study on Measurement Methods of Bulk Density and Porosity of Rock Samples. Journal of Geoscience and Environment Protection 3, 72-79.

Linke, P., Lutze, G.F., 1993. Microhabitat preferences of benthic foraminifera a static concept or a dynamic adaptation to optimize food acquisition? Marine Micropaleontology 20, 215-234.

Llave, E., Hernández-Molina, F.J., Somoza, L., Díaz-del-Río, V., Stow, D.A.V., Maestro, A., Alveirinho Dias, J.M. 2001. Seismic stacking pattern of the Faro-

Albufeira contourite system (Gulf of Cadiz): a Quaternary record of paleoceanographic and tectonic influences. Marine Geophysical Researches 22, 487-508.

Llave, E., Hernández-Molina, F.J., Somoza, L., Stow, D.A.V., Díaz del Río, V., 2007, Quaternary evolution of the contourite depositional system in the Gulf of Cadiz. In: Viana, A., Rebesco, M. (Eds.) Economic and Paleoceanographic Importance of Contourites. Geological Society, London, Special Publication 276, 49-79.

Lobo, F.J., Hernandez-Molina, F.J., Somoza, L., Rodero, J., Maldonado, A., Barnolas, A., 2000. Patterns of bottom current flow deduced from dune asymmetries over the Gulf of Cadiz shelf (southwest Spain). Marine Geology 164, 91-117.

Lobo, F.J., Maldonado, A., Noormets, R., 2010. Large-scale sediment bodies and superimposed bedforms on the continental shelf close to the Strait of Gibraltar: interplay of complex oceanographic conditions and physiographic constraints. Earth Surface Processes and Landforms 35, 663-679.

Longhitano, S.G., 2013. A facies-based depositional model for ancient and modern, tectonically–confined tidal straits. Terra Nova 25, 446-452.

Longhitano, S.G., Mellere, D., Steel, R.J., Ainsworth, R.B., 2012. Tidal depositional systems in the rock record: a review and new insights. Sedimentary Geology 279, 2-22.

Longhitano, S.G., Chiarella, D., Muto, F., 2014. Three-dimensional to two-dimensional cross-strata transition in the lower Pleistocene Catanzaro tidal strait transgressive succession (southern Italy). Sedimentology 61, 2136-2171.

Lourens, L., Hilgen, F.J., Laskar, J., Shackleton, N.J., Wilson, D., 2004. The Neogene Period. In: Gradstein, F., Ogg, J., and Smith, A. (Eds.), A Geologic Time Scale, Cambridge University Press, London, pp. 409–440.

Lovell, J.P.B., Stow, D.A.V., 1981. Identification of ancient sandy contourites. Geology 9, 347-349.

Lutze, G.F., Coulbourn, W.T., 1984. Recent benthic foraminifera from the continental margin of northwest Africa: community structure and distribution. Marine Micropaleontology 8, 361-401.

Masson, D.G., Wynn, R.B., Bett, B.J., 2004. Sedimentary environment of the Faeroe Shetland Channel and Faeroe Bank channels, NE Atlantic, and the use of bedforms as indicators of bottom current velocity in the deep ocean. Sedimentology 51, 1–35.

Mauritzen, C., 1996. Production of dense overflow waters feeding the North Atlantic across the Greenland-Scotland Ridge. Part 1: Evidence for a revised circulation scheme. Deep Sea Research Part I: Oceanographic Research Papers 43, 769-806.

Middleton, G. V., Southard, J. B., 1984. Mechanics of sediment transport, 2nd edition. Society of Economic Paleontologists and Mineralogists, Eastern Section Short Course 3, Providence, RI.

Mitchell, N., Masselink, G., Huthance, J.M., Fernández-Sañas, L.M., Lobo, F.J., 2012. Depths of Modern Coastal Sand Clinoforms. Journal of Sedimentary Research 82(7):469-481.

Münch, P., Martín , J. J., Feraud, G., Saint-Martin, J. P., Ferrandini, M., Garcia, F., Conesa, G., Roger, S., Moullade, M., 2006, Precise Ar-40/Ar-39 dating of volcanic tuffs within the upper Messinian sequences in the Melilla carbonate complex (NE Morocco): implications for the Messinian Salinity Crisis: International Journal of Earth Sciences 95, 491-503.

Murray, J.W., 2006. Ecology and Applications of Benthic Foraminifera. Cambridge University Press, London.

Mutti, E., Normark, W.R., 1987. Comparing examples of modern and ancient turbidite systems: problems

and concepts. In: Leggett, J.K., Zuffa, G.G. (Eds.), Marine Clastic Sedimentology: Concepts and Case Studies. Springer Netherlands, Dordrecht, pp. 1–38.

Mutti, E., Tinterri, R., Benevelli, G., di Biase, D., Cavanna, G., 2003. Deltaic, mixed and turbidite sedimentation of ancient foreland basins. Marine and Petroleum Geology 20, 733-755.

Nachite, D., Bekkali, R., Rodríguez Lázaro, J., Martín Rubio, M., 2003. Los ostrácodos lacustres del Plioceno superior de la Cuenca de Saïss (Norte de Marruecos): Principales características palaeoambientales. Geogaceta 34, 95-98.

Naranjo, C., Sammartino, S., García-Lafuente, J., Bellanco, M.J., Taupier-Letage, I., 2015. Mediterranean waters along and across the Strait of Gibraltar, characterization and zonal modification. Deep Sea Research Part I: Oceanographic Research Papers 105, 41-52.

Nelson, C.H., Baraza, J., Maldonado, A., 1993. Mediterranean undercurrent sandy contourites, Gulf of Cadiz, Spain. Sedimentary Geology 82, 103-131.

Nelson, C.H., Baraza, J., Rodero, J., Maldonado, A., Escutia, C., Barber, Jr. J.H. 1999. Influence of the Atlantic inflow and Mediterranean outflow currents on Late Pleistocene and Holocene

sedimentary facies of Gulf of Cadiz continental margin. Marine Geology 155, 99-129.

Nemec, W., 1988. The shape of the rose. Sedimentary Geology 59, 149-152.

Nielsen, T., Knutz, P.C., Kuijpers, P.C.A., 2008. Seismic expression of contourite depositional systems. In: Rebesco, M., Camerlenghi, A. (Eds.), Contourites, Developments in Sedimentology 60. Elsevier, Amsterdam, pp. 301–322.

Olariu, C., Steel, R.J., Dalrymple, R.W., Gingras, M.K., 2012. Tidal dunes versus tidal bars: the sedimentological and architectural characteristics of compound dunes in a tidal seaway, the lower Baronia Sandstone (Lower Eocene), Ager Basin, Spain. Sedimentary Geology 279, 134-155.

Payton, C. E., 1977, Seismic stratigraphy: Applications to hydrocarbon exploration. AAPG Memoir 26, 516 p.

Pérez-Asensio, J. N., Aguirre, J., Schmiedl, G., Civis, J., 2012. Messinian palaeoenvironmental evolution in the lower Guadalquivir Basin (SW Spain) based on benthic foraminifera. Palaeogeography, Palaeoclimatology, Palaeoecology 326, 135-151.

Platt, J.P., Allerton, S., Kirker, A., Mandeville, C., Mayfield, A., Platzman, E.S., Rimi, A., 2003. The ultimate arc: Differential displacement, oroclinal

bending, and vertical axis rotation in the External Betic-Rif arc. Tectonics 22.

Rebesco, M., Hernández-Molina, F. J., Van Rooij, D., Wåhlin, A, 2014. Contourites and associated sediments controlled by deep-water circulation processes: state of the art and future considerations. Marine Geology 352, 111-154.

Rogerson, M., Bigg, G. R., Rohling, E. J., Ramirez, J., 2012. Palaeoceanography of the Atlantic-Mediterranean exchange: Overview and first quantitative assessment of climatic forcing. Reviews of Geophysics 50.

Roksandic, M.M., Soquip, J., 1990. Geology and Hydrocarbon Potential of the Rharb Basin, Morocco [Abstract]. Bulletin of Canadian Petroleum Geology 38, 178-178.

Roveri, M., Flecker, R., Krijgsman, W., Lofi, J., Lugli, S., Manzi, V., Sierro, F.J., Bertini, A., Camerlenghi, A., De Lange, G., Govers, R., Hilgen, F.J., Hübscher, C., Meijer, P.T., Stoica, M., 2014. The Messinian Salinity Crisis: Past and future of a great challenge for marine sciences. Marine Geology 352, 25-58.

Saidova, K.M., 2008. Foraminifer Communities of the Atlantic Continental Margin of Europe. Oceanology 48, 217-227.

Saint-Martin, J.P., Charrière, A., 1989. Les édifices coralliens marqueurs de l'évolution paléogéographique en bordure du Moyen Atlas (Maroc). Sciences Géologiques, Strasbourg, Mémoire 84, 83-94.

Saint-Martin, J.P., Cornée , J.J., 1996. The Messinian reef complex of Melilla, northeastern Rif, Morocco. Models for Carbonate Stratigraphy from Miocene Reef Complexes of Mediterranean Regions. In: Franseen, E.K., Esteban, M., Ward, W.C., Rouchy, J.M. (Eds.), Society of Economic Paleontologists and Mineralogists, Concepts in Sedimentology and Palaeontology 5, 227–237.

Sammartino, S., García Lafuente, J., Naranjo, C., Sánchez Garrido, J.C., Sánchez Leal, R., Sánchez Román, A., 2015. Ten years of marine current measurements in Espartel Sill, Strait of Gibraltar. Journal of Geophysical Research: Oceans 120, 6309-6328.

Sani, F., Del Ventisette, C., Montanari, D., Bendkik, A., Chenakeb, M., 2007. Structural evolution of the Rides Prerifaines (Morocco): structural and seismic interpretation and analogue modelling experiments. International Journal of Earth Sciences 96, 685-706.

Santoro, V.C., Amore, E., Cavallaro, L., Cozzo, G., Foti, E., 2002. Sand waves in the Messina strait, Italy. Journal of Coastal Research 36, 640-653.

Scher, H.D., Martin, E.E., 2006. Timing and climatic consequences of the opening of Drake Passage. Science 312, 428-430.

Schönfeld, J., 1997. The impact of the Mediterranean Outflow Water (MOW) on benthic foraminiferal assemblages and surface sediments at the southern Portuguese continental margin. Marine Micropalaeontology 29, 211-236.

Schönfeld, J., 2002. Recent benthic foraminiferal assemblages in deep high-energy environments from the Gulf of Cadiz (Spain). Marine Micropalaeontology 44, 141-162.

Schönfeld, J., Zahn, R., 2000. Late glacial to Holocene history of the Mediterranean outflow. Evidence from benthic foraminiferal assemblages and stable isotopes at the Portuguese margin. Palaeogeography, Palaeoclimatology, Palaeoecology 159, 85–111.

SCP/ERICO report, 1991. Etude de synthèse géologique et géophysique du bassin du Gharb. ONHYM internal report, London, 533 pp.

Shanmugam, G., Spalding, T.D., Rofheart, D.H., 1993. Process sedimentology and reservoir quality of deep-marine bottom-current reworked sands

(sandy contourites): an example from the Gulf of Mexico. AAPG Bulletin 77, pp.1241-1259.

Shanmugam, G., 2006. Deep-water Processes and Facies Models: Implications for Sandstone Petroleum Reservoirs. Handbook of Petroleum Exploration and Production 5. Elsevier, Amsterdam.

Sierro, F.J., 1985. The replacement of the "Globorotalia menardii" group by the Globorotalia miotumida group: an aid to recognizing the Tortonian/Messinian boundary in the Mediterranean and adjacent Atlantic. Marine Micropaleontology 9, 525-535.

Sierro, F.J., Flores, J.A., Civis, J., Gonza, J.A., France, G., 1993. Late Miocene globorotaliid event-stratigraphy and biogeography in the NE-Atlantic and Mediterranean. Marine Micropalaeontology 21, 143-167.

Sierro, F. J., Hilgen, F. J., Krijgsman, W., Flores, J. A., 2001. The Abad composite (SE Spain): a Messinian reference section for the Mediterranean and the APTS. Palaeogeography, Palaeoclimatology, Palaeoecology 168, 141-169.

Sinclair, H.D., 1997. Tectonostratigraphic model for underfilled peripheral foreland basins: An Alpine perspective. Geological Society of America Bulletin 109, 324-346.

Sprovieri, R., Di Stefano, E., Sprovieri, M., 1996. High resolution chronology for Late Miocene Mediterranean stratigraphic events. Rivista Italiana di Paleontologia e Stratigrafia 102, 77-104.

Sprovieri, M., Bellanca, A., Neri, R., Mazzola, S., Bonanno, A., Patti, B., Sorgente, R., 1999. Astronomical calibration of late Miocene stratigraphic events and analysis of precessionally driven paleoceanographic changes in the Mediterranean basin. Memorie della Società Geologica Italiana 54, 7-24.

Stow, D.A.V., 1985. Fine-grained sediments in deep water: An overview of processes and facies models. Geo-Marine Letters 5, 17-23.

Stow, D.A.V., 2005. Sedimentary rocks in the field: a colour guide. Manson Publishing, London.

Stow, D.A.V., Tabrez, A., 1998. Hemipelagites: facies, processes and models. Geological Society, London, Special Publication 129, 317-338

Stow, D.A.V., Johansson, M., 2000. Deep-water massive sands: nature, origin and hydrocarbon implications. Marine and Petroleum Geology 17, 145-174.

Stow, D.A.V., Faugères, J.C., 2008. Contourite facies and the facies model. Developments in Sedimentology 60, 223-256.

Stow, D.A.V., Faugères, J.-C., Viana, A., Gonthier, E., 1998. Fossil contourites: a critical review. Sedimentary Geology 115, 3–31.

Stow, D.A.V., Hernández-Molina, F.J., Llave, E., Sayago-Gil, M., del Río, V.D., Branson, A., 2009. Bedform-velocity matrix: the estimation of bottom current velocity from bedform observations. Geology 37, 327-330.

Stow, D.A.V., Hernández-Molina, F.J., Llave, E., Bruno, M., García, M., del Rio, V.D., Somoza, L., Brackenridge, R.E., 2013. The Cadiz Contourite Channel: Sandy contourites, bedforms and dynamic current interaction. Marine Geology 343, 99-114.

Stride, A.H., 1982. Offshore tidal deposits: sand sheet and sand bank facies. In: Stride, A.H. (Ed.), Offshore Tidal Sands: Processes and Deposits. Springer Netherlands, Dordrecht, pp. 95-125.

Surlyk, F., Noe-Nygaard, N., 1992. Sand bank and dune facies architecture of a wide intracratonic seaway: late Jurassic-early Cretaceous Raukelv Formation, Jameson Land, east Greenland. In: Miall, A.D., Tyler, N. (Eds.), The Three-dimensional Facies Architecture of Terrigenous Clastic Sediments, and its Implications for Hydrocarbon Discovery and Recovery. Concepts in Sedimentology and Paleontology 3, pp. 261-276.

Suter, G., 1980. Carte géologique de la Chaine Rifaine, échelle 1:500.000. Ministère de l'Energie et des Mines du Maroc, Direction de la Géologie, Rabat, Notes et Mémoires du Service Géologique du Maroc 245a.

Swift, J.H., 1984. The circulation of the Denmark Strait and Iceland-Scotland overflow waters in the North Atlantic. Deep Sea Research Part A. Oceanographic Research Papers 31, 1339-1355.

Tinterri, R., 2011. Combined flow sedimentary structures and the genetic link between sigmoidal-and hummocky-cross stratification. GeoActa 10, 43–85.

Tucker, M.E., 2011. Sedimentary rocks in the field: a practical guide. Wiley-Blackwell, Chichester, pp. 276..

Van der Laan, E., Snel, E., De Kaenel, E., Hilgen, F.J., Krijgsman, W., 2006. No major deglaciation across the Miocene–Pliocene boundary: integrated stratigraphy and astronomical tuning of the Loulja sections (Bou Regreg area, NW Morocco). Paleoceanography 21, 1-27.

Van der Zwaan, G.J., Jorissen, F.J., De Stigter, H.C., 1990. The depth dependency of planktonic/benthic foraminiferal ratios: Constraints and applications. Marine Geology 95, 1-16.

Vergés, J., Fernàndez, M., 2012. Tethys–Atlantic interaction along the Iberia–Africa plate boundary: The Betic–Rif orogenic system. Tectonophysics 579, 144-172.

Visser, M.J., 1980. Neap-spring cycles reflected in Holocene subtidal large-scale bedform deposits: a preliminary note. Geology 8, 543-546.

Wernli, R., 1988. Micropaléontologie du Néogène post-nappes du Maroc septentrional et description systématique des foraminifères planctoniques. Notes et Mémoires du Service Géologique du Maroc 331, 1-266.

Zizi, M., 1996. Triassic–Jurassic extension and Alpine inversion in the northern Morocco, in: Ziegler, P.A., Horvath, F. (Eds.), Peri-Tethys Memoir 2: Structure and prospects of the Alpine basins and forelands. Mémoires du Muséum National d'Histoire Naturelle 170, Paris, pp. 87-101.

Zizi, M., 2002. Triassic-Jurassic extensional systems and their Neogene reactivation in Northern Morocco (the Rides Prerifaines and Guercif basin). Notes et Mémoires du Service Géologique du Maroc 416, 1-138.

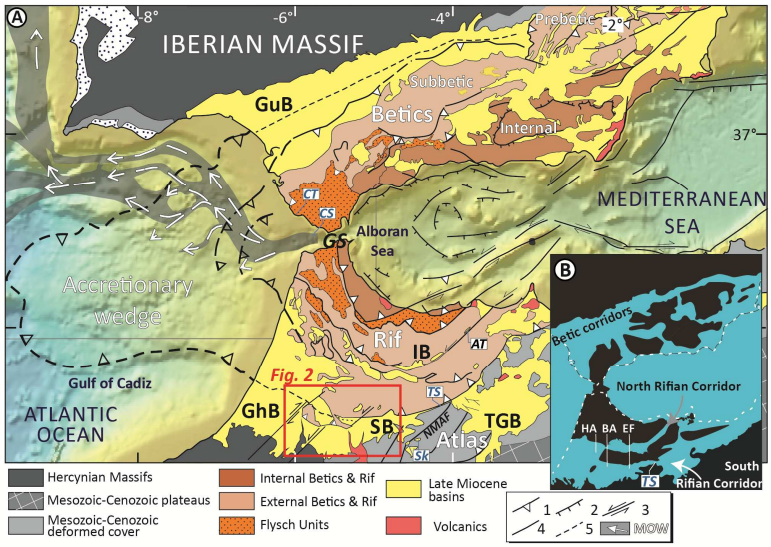

Figure 1

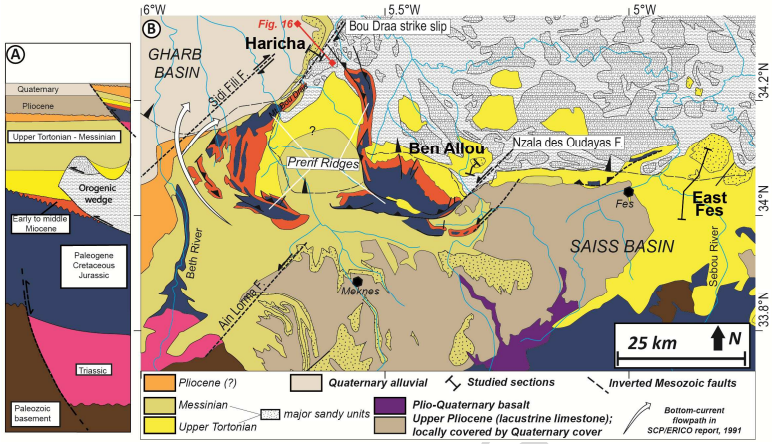

Figure 2

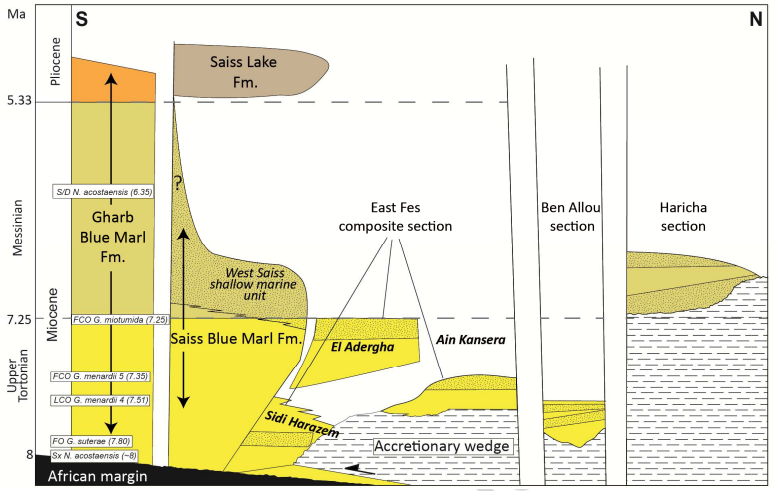

Figure 3

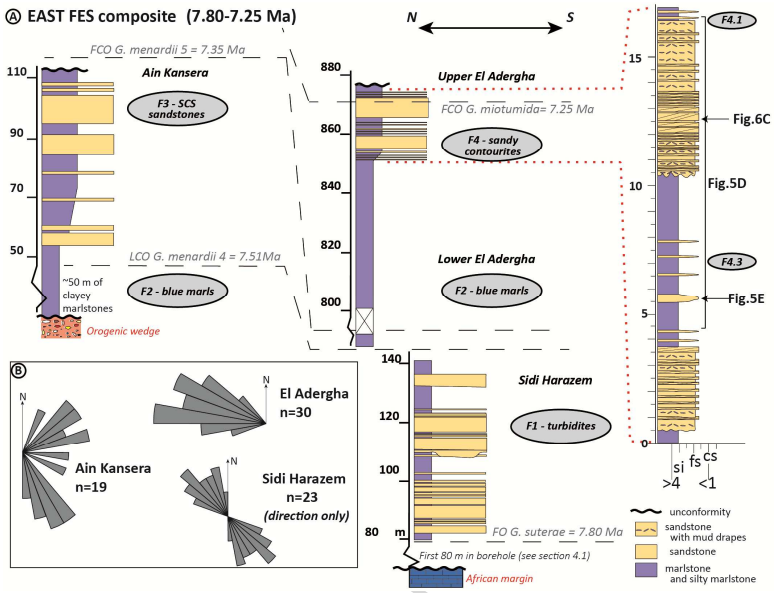

Figure 4

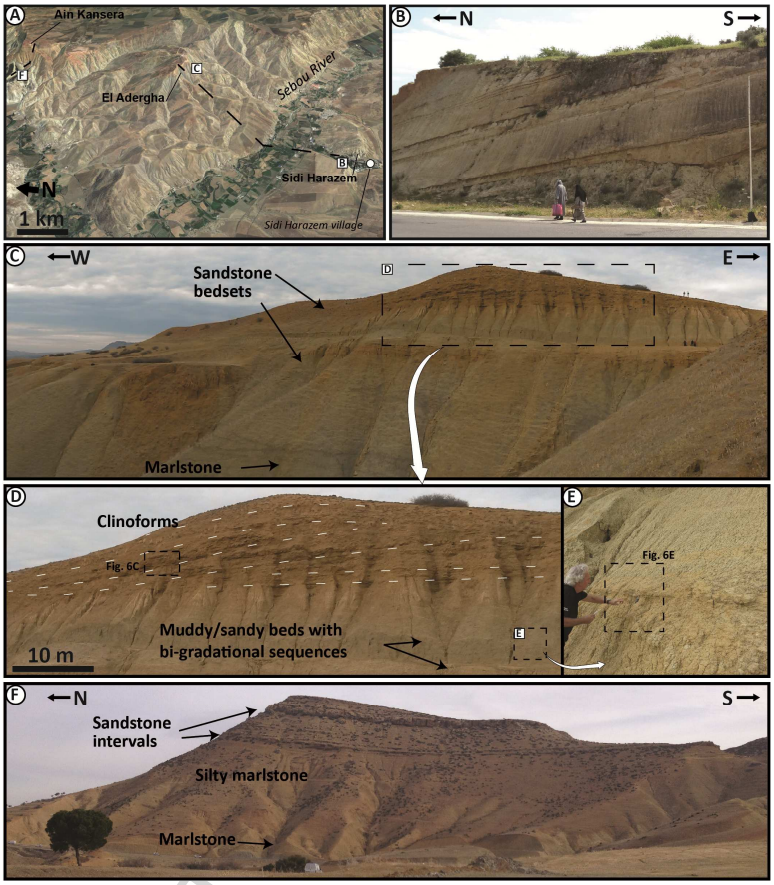

Figure 5

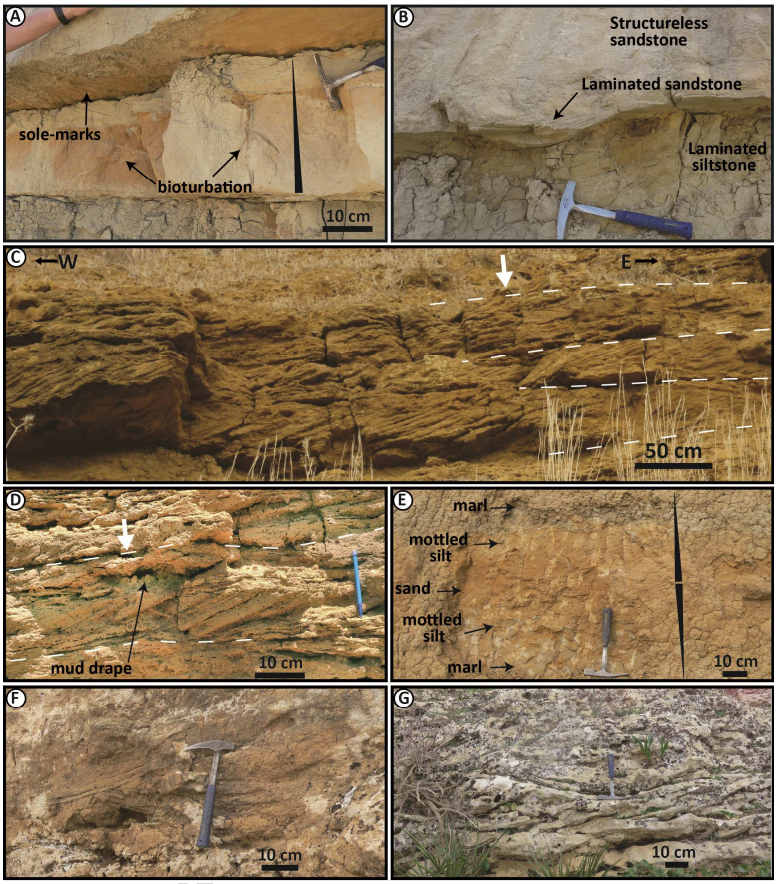

Figure 6

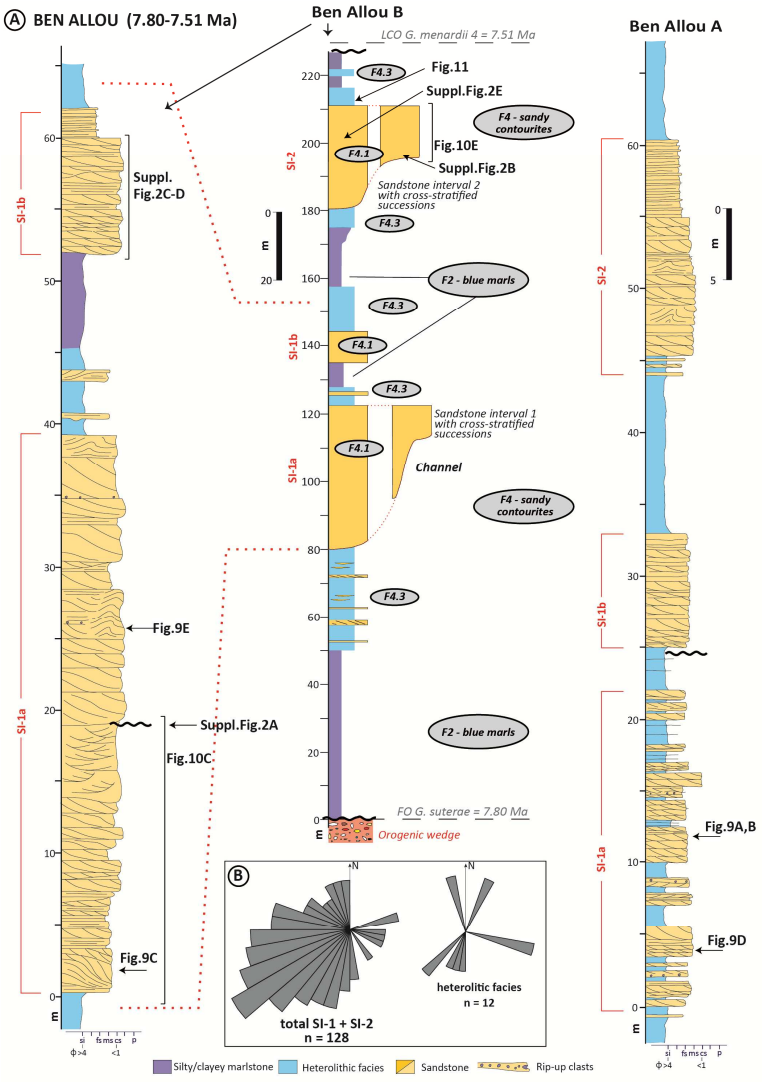

Figure 7

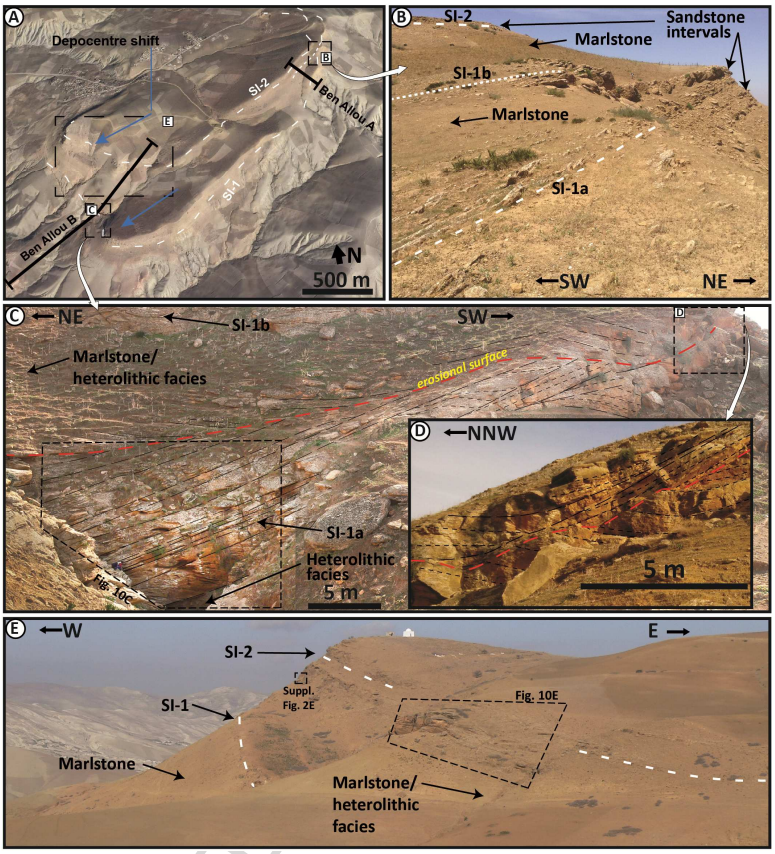

Figure 8

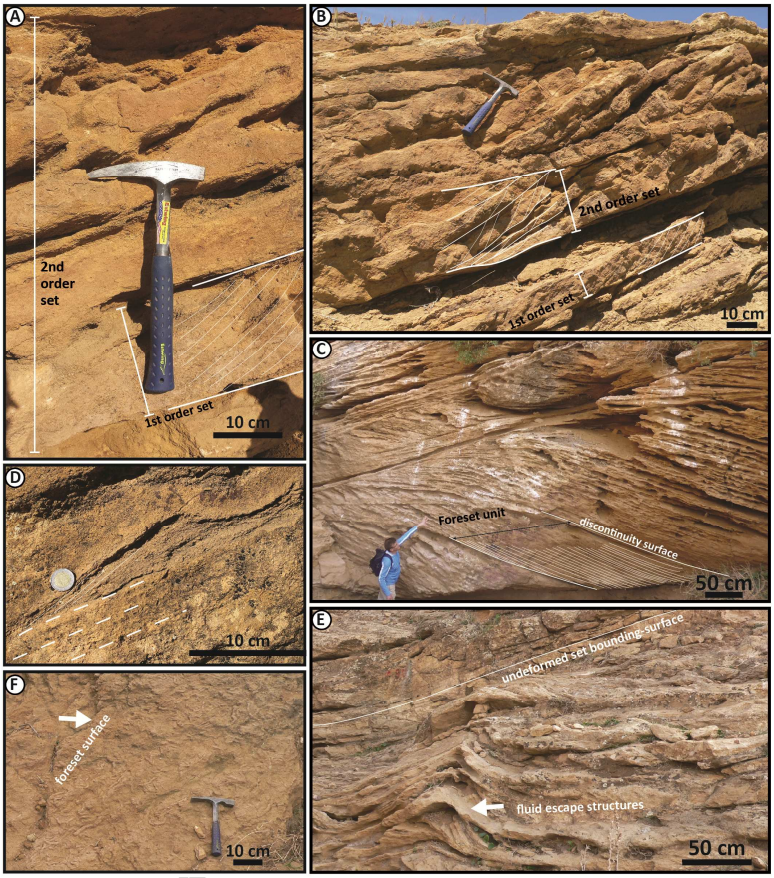

Figure 9

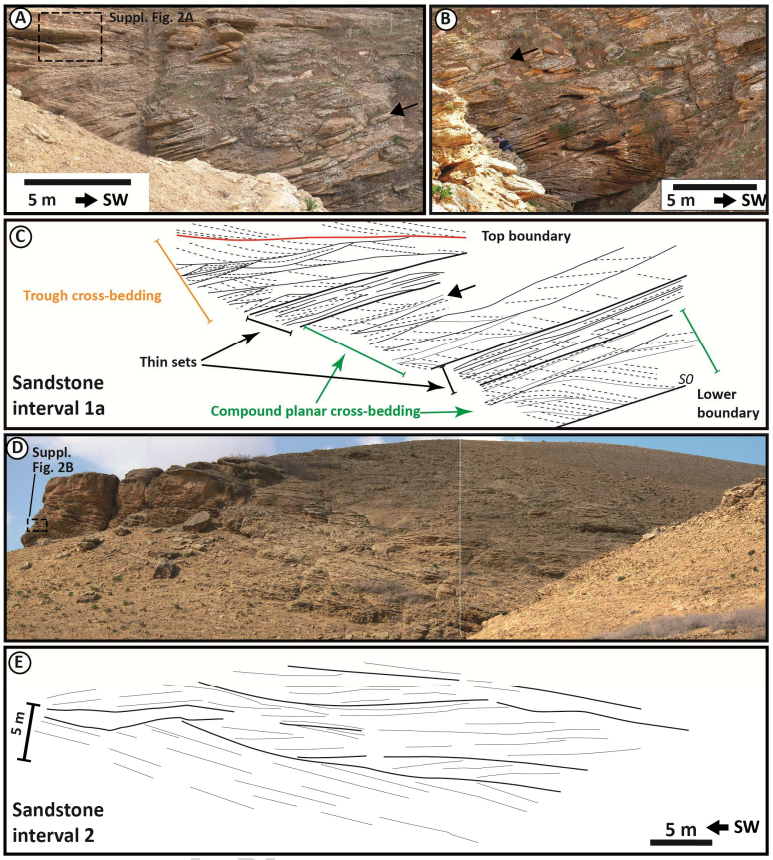

Figure 10

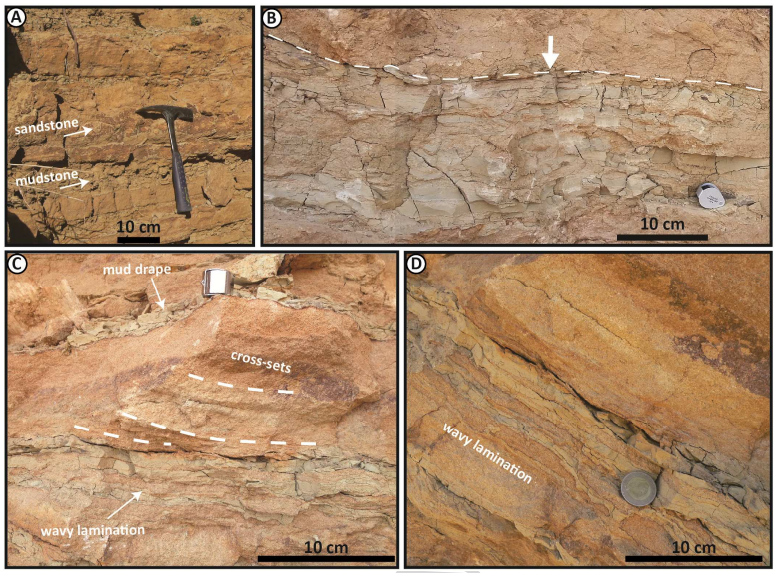

Figure 11

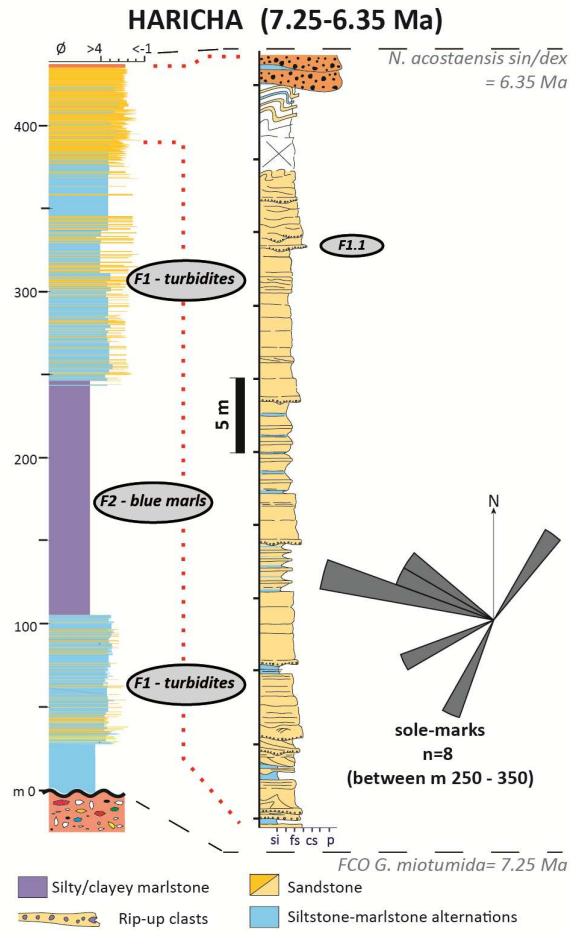

Figure 12

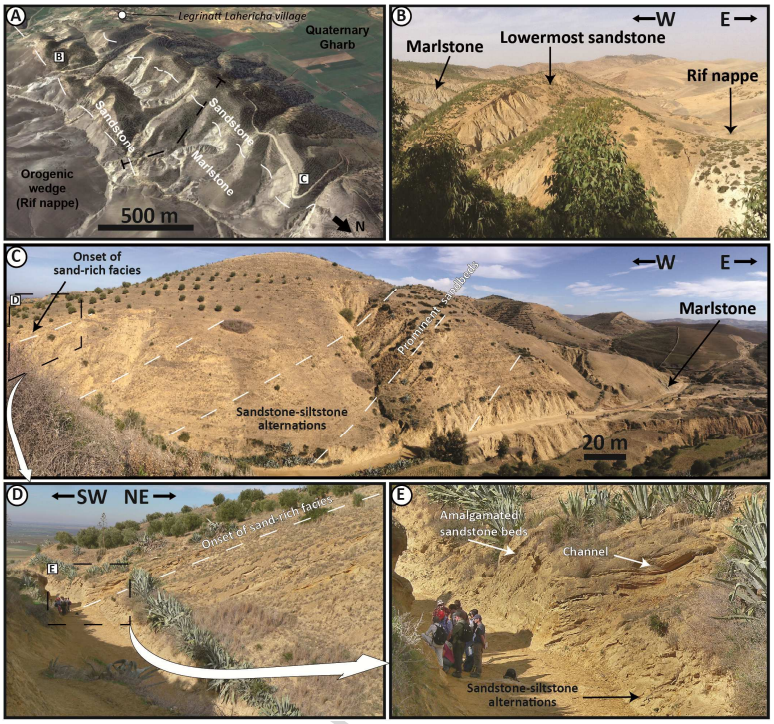

Figure 13

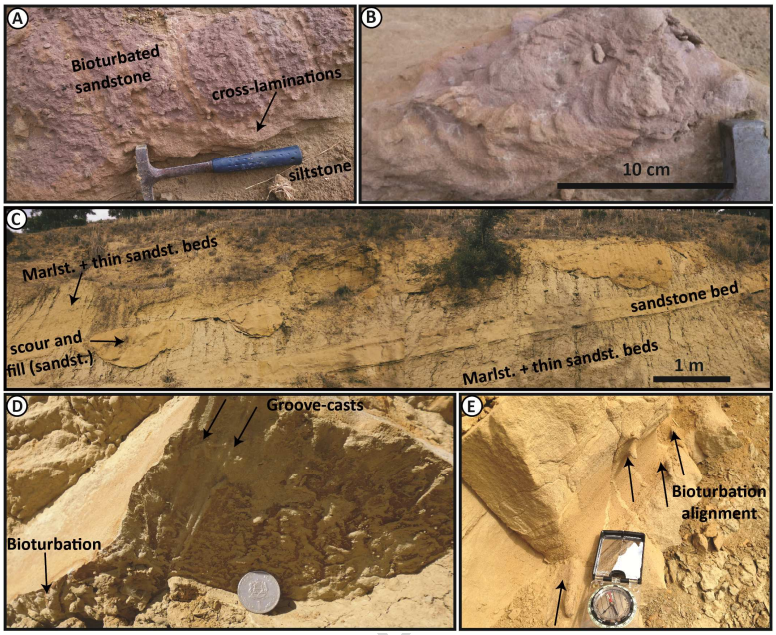

Figure 14

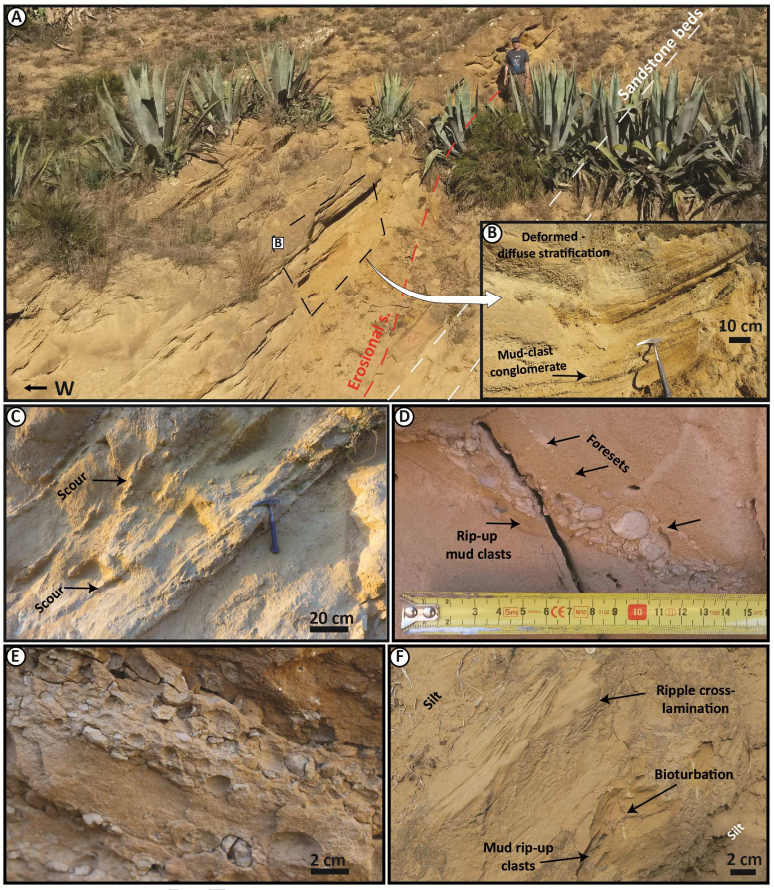

Figure 15

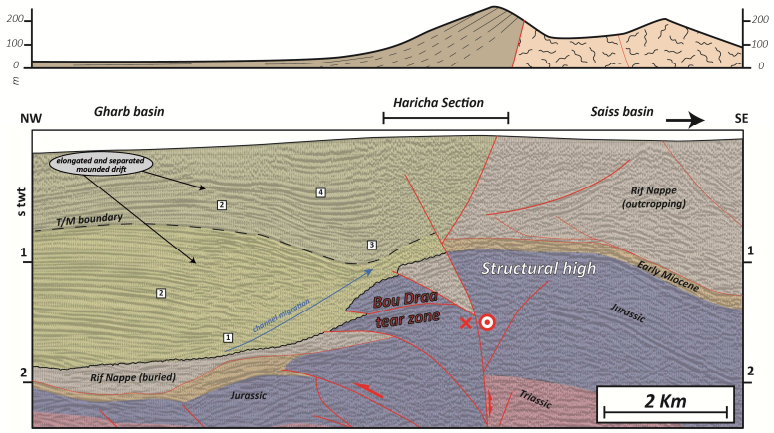

Figure 16

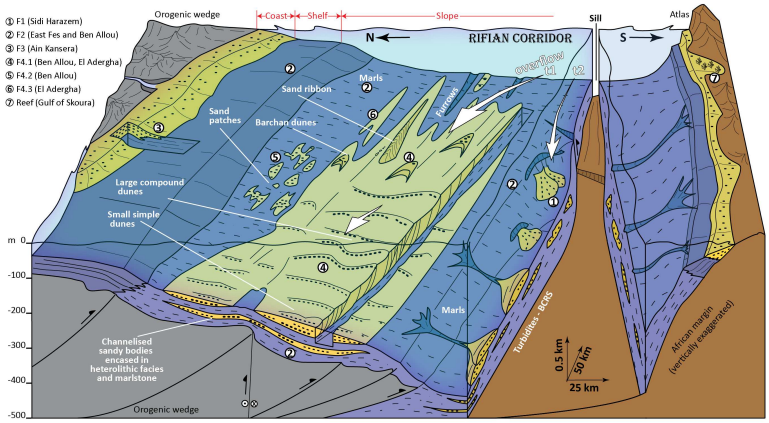

Figure 17

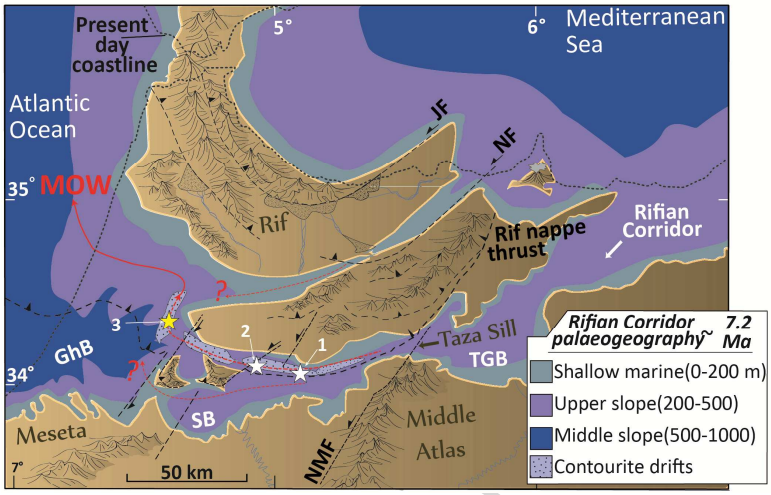

Figure 18

Table 1

	Facies	Section (age)	Lithology	Structures	Thickness	Geometry	Mechanism of formation	Palaeo-water depth (m)	Possible processes	References
Facies association F1	Normally graded, structureless to crudely laminated sandstone	Sidi Harazem (7.80 - 7.51 Ma) Haricha (7.25 - 6.35 Ma)	Poorly to moderately sorted fine to coarse sandstone	Linear solemarks and load-casts; abundant burrows and ichnofacies (e.g., Zoophycus, Chondrites, Rhizocorallium)	0.05 - 4 m thick	Sheet-like beds with sharp to erosive bases; local channels or scours 0.1-10 m wide, 0.1-2 m deep	Nearbed suspension generated by sand-laden turbidity current	250 - 400 (Sidi Harazem) 150 - 250 (Haricha)		
	Ripple laminated sandstone	Sidi Harazem (7.80 - 7.51 Ma) Haricha (7.25 - 6.35 Ma)	Fine to coarse sandstone	Asymmetrical ripples in single sets	1 - 5 cm thick	Sheet-like or laterally confined divisions	Predominant traction and resuspension	idem	Proximal turbidity currents in foreland basins; transition from sandy debris flows into fully turbulent flow. High river input and sediment failures possibly driven by tectonic uplift of the seaway margins	e.g., Stow, 1985; Mutti et al., 2003
	Plane-parallel laminated sandstone	Sidi Harazem (7.80 - 7.51 Ma) Haricha (7.25 - 6.35 Ma)	Fine to coarse sandstone	Plane parallel to sub-horizontal lamination; moderate amount of bioturbation (e.g., Planolites and Thalassinoides)	1 - 5 cm thick	Horizontal divisions in sheet-like beds	Low rate of suspended sedimentation, predominant traction and resuspension	idem		
	Bioturbated siltstone to marlstone	Sidi Harazem (7.80 - 7.51 Ma) Haricha (7.25 - 6.35 Ma)	Marlstone and siltstone	Variable amount of bioturbation (e.g., Planolites, Thalassinoides, Zoophycus) fossil debris (e.g., bivalves and echinoderms)	0.5 - 1 m thick	Sub-horizontal divisions in sheet-like beds	Waning flow	idem		

F1.1	Massive and deformed sandstone with abundant mudclasts	Haricha (7.25 - 6.35 Ma)	Fine to medium sandstone with variable amount of silt	Abundant scours, plane parallel lamination, liesegang rings, sediment deformation; rip-up and floating mudclasts such as: isolated floating clasts, clustered floating clasts, ordered stratified clasts	Single bed ~2 m thick; amalgamated beds up to ~10 m thick	Channelised (lobe) geometry at the base	Sandy debris flow with channel-margin collapse or headward slumping. Traction as the base of the flow in high-concentration turbidity currents	150 - 250	Mass flow events channelised in trough-conduits	Liesegang rings: Stow, 2005; Tucker, 2011 Deep water massive sands: Johansson and Stow, 1995; Stow and Johansson, 2000; Haughton et al., 2009
	Matrix-supported mudclast conglomerate	Haricha (7.25 - 6.35 Ma)	Fine to medium sand (matrix) and mudstone clasts	Plane parallel and cross lamination; diffuse stratification	0.1 - 0.5 m thick	Sheet-like geometry or lenses	Cohesive sandy debris flow	150 - 250		
F2	Massive to crudely laminated marlstone or mudstone	All units (7.80 - 6.35 Ma)	Marlstone, silty marlstone mudstone	Variable amount of bioturbation (Cruziana); fossil debris (e.g., bivalves and echinoderms)	Facies exposure: 5 to 700 m thick	Pinch-out landward (basin scale)	(a) Flocculation and settling (b) Far-travelled particles, deposited from suspension	50-100 (Ain Kansera) 250-400 (Sidi Harazem) 150 - 400 (El Adergha) 150-400 (Ben Allou) 150-250 (Haricha)	(a) Hemipelagic processes (b) Bottom-current	(a) Stow and Tabrez, 1998; Hüneke and Henrich, 2011 (b) Stow and Faugères, 2008; Rebesco et al., 2014
F3	Amalgamated bioclastic sandstone with SCS	Ain Kansera (7.51 - 7.35 Ma)	Medium to very coarse sandstone	Troughs 20–50 cm deep and 50–100 cm wide; concave upward scours covered by foresets with the same angle of the basal erosive surface; skolithos ichnofacies	0.5 - 5 m thick	Sheet-like beds	Aggrading hummocky beds under oscillatory current with no (or weak) unidirectional currents	15 - 50	(a) Wave/storm action in coastal environment (b) Hyperpycnal flows resulting in delta-front sandstone lobes	(a) Leckie and Walker, 1982; Dumas and Arnott, 2006 (b) Mutti et al., 2003; Tinterri, 2011

F4	Bioclastic and unidirectional crossbedded sandstone	Ben Allou (7.80 - 7.51 Ma) El Adergha (7.35 - 7.25 Ma)	Fine to coarse sandstone	Westward oriented foresets; variety of cross-stratification shown in Table 2; dewatering structures; abundant bioturbation (Planolites)	Facies exposure: 5 to 40 m thick; cross-sets (single or compound): 0.1 to 15 m thick	Sheet-like beds; channel infills (50 m wide and 15 m deep incisions at the base of parasequence S1, Table 2); wedges (pinch-out toward controlling fault)	Migrating dune field under unidirectional flow (Table 2). Flow v > 0.5 m/s	150 - 300	(a) predominantly unidirectional currents in a narrow strait, tidal/bottom current influence (b) bottom-current passage through narrow seaway, may have deep tidal influence	(a) Anastas et al., 1997, 2006; Longhitano, 2013 (b) Rebesco et al., 2014; Hernández-Molina et al., 2016c; Ercilla et al., 2017
	Laminated heterolithics	Ben Allou (7.80 - 7.51 Ma)	Fine to medium sandstone with alternating mudstone separated locally by thin veneers of siderite bands	Wavy lamination; asymmetrical dune cross-sets up to 15 cm thick; scattered pattern of foreset orientations; moderate bioturbation (Planolites)	Facies exposure: 2 to 50 m thick; mud layers: 0.5 to 5 cm thick; sand layers: 2 to 20 cm thick	Generally structureless sandstone with variable bioclastic content; laterally continuous or pinching-out subhorizontal layers	Alternating traction and resuspension. Decelerating velocity in mixed muddy/sandy flow	150 - 300	Deceleration of the dominant unidirectional current. Lower suspended sediment concentration. Sand patches and rippled sand sheets along a sediment transport path	Belderson et al., 1982; Stow et al., 2009; Rebesco et al., 2014; Baas et al., 2016
	Sandstone-mudstone units with bi-gradational sequences	El Adergha (7.35 - 7.25 Ma)	Marlstone, siltstone, and fine to medium sandstone	Gradational sandstone bed contacts with irregular grading (both normal and inverse); burrowed sandstone; mottled siltstone; indistinct to plane-parallel lamination	0.1 - 1 m thick	Sheet-like geometry	Gradual changes in current strength; resuspension and deposition. Flow v < 0.5 m/s	150 - 300	Mainly depositional, low-energy bottom currents; possible interbedded hemipelagic sedimentation	Stow et al., 1998; Stow and Faugères, 2008; Rebesco et al., 2014

Table 2

Code	Type of structure	Type of bedform	Internal Organization	Cross-set thickness	Bounding surface	Shape of Internal strata (threshold = >40 ° variation)	Accretion direction	Mechanism of formation
L1	Cross-lamination with straight cross-strata	Ripples	Simple	2-6 cm	Planar	Straight	Forward	Traction, grainfall, grainflow
L2	Cross-lamination with sinuous cross-strata	Ripples	Simple	2-6 cm	Planar to trough	Sinuous	Forward	Traction, grainfall, grainflow
B1	Simple Cross-bedding with angular cross-strata	Dunes	Simple	10 - 500 cm (Ben Allou) 10 - 50 cm (El Adergha)	Planar	Straight	Forward	Migration of straight and sinuous crested dunes without lee-superimposed dunes
B2	Simple, tabular cross-bedding with sinuous cross-strata	Dunes	Simple	10 - 250 cm	Planar to trough	Sinuous	Forward	Same as **B1** except higher velocity
B3	Trough cross-bedding with sinuous cross-strata	Dunes	Compound	10 - 250 cm	Trough	Sinuous	Forward	Same as **B2** except higher velocity
B4	Compound cross-bedding with straight to sinuous cross-strata	Dunes	Compound	10 - 250 cm	Planar	Straight to sinuous	Forward	Migration of compound dunes, or dunes affected by flow fluctuation

S1	Horizontally-bedded cross stratified succession	Migrating dune field	Simple to compound	5 to 15 m	Planar	Tabular, stratiform bodies	Vertical	Migration of a dune field, composed by simple and compound dunes under constant flow with fluctuation in velocity
S2	Cross-stratified succession with downcutting clinoforms	Migrating dune field	Compound	5 to 15 m	Planar to slightly inclined	Sinuous, tabular and wedge-shaped	Vertical and down-flow	Migration of a dune field, composed by simple and compound dunes under waning flow